Published in final edited form as:

Biochem J. 2021 March 26; 478(6): 1261–1282. doi:10.1042/BCJ20200984.

FoxA2 and RNA Pol II Mediate Human Islet Amyloid Polypeptide Turnover in ER-stressed Pancreatic β-cells

Diti Chatterjee Bhowmick[†], **Lydia Burnett**, **Zhanar Kudaibergenova**, **Aleksandar M. Jeremic**[*]

Department of Biological Sciences, The George Washington University, 800 22nd Street, N.W., Washington D.C. 20052, U.S.A

Abstract

Here, we investigated transcriptional and trafficking mechanisms of human islet amyloid polypeptide (hIAPP) in normal and stressed β-cells. In high glucose-challenged human islets and rat insulinoma cells overexpressing hIAPP, cell fractionation studies revealed increased accumulation of hIAPP. Unexpectedly, a significant fraction (up to 22%) of hIAPP was found in the nuclear soluble and chromatin-enriched fractions of cultured human islet and rat insulinoma cells. The nucleolar accumulation of monomeric forms of hIAPP did not have any adverse effect on the proliferation of β-cells nor did it affect nucleolar organization or function. However, intact nucleolar organization and function were essential for hIAPP expression under normal and ER-stress conditions as RNA polymerase II inhibitor, α-amanitin, reduced hIAPP protein expression evoked by high glucose and thapsigargin. Promoter activity studies revealed the essential role of transcription factor FoxA2 in hIAPP promoter activation in ER-stressed β-cells. Transcriptome and secretory studies demonstrate that the biosynthetic and secretory capacity of islet β-cells was preserved during ER stress. Thus, the main reason for increased intracellular hIAPP accumulation is its enhanced biosynthesis under these adverse conditions.

Keywords

Islet amyloid polypeptide; ER stress; transcription; FoxA2; trafficking; nucleolus

INTRODUCTION

Eukaryotic cells consist of several membrane-bound organelles and an elaborate endomembrane system (1). Each organelle provides a distinct compartment for specific cellular functions. As the cytosol is the major site for protein translation, a majority of the newly synthesized proteins are trafficked into one or more cellular organelles in order to

[*]**Correspondence:** Aleksandar Jeremic, Ph.D., Department of Biological Sciences, George Washington University, Washington D.C. 20052; jerema@gwu.edu; Tel. (202) 994-7899; Fax. (202) 994-610.

[†]**Present address**: Dept. of Molecular and Cellular Endocrinology, Arthur Riggs Diabetes and Metabolism Research Institute, City of Hope's Beckman Research Institute, 1500E Duarte Road, Duarte, CA 91010.

Data Availability

All primers used for qPCR experiments are provided in supporting information. 3D confocal images used in movies S1/S2 are available from the corresponding author upon request.

Competing Interests

The authors declare that they have no competing interests with the contents of this article.

achieve their functional destination (1, 2). Therefore, proper cellular trafficking and subcellular localization of newly synthesized proteins are essential for maintaining cellular homeostasis (1). Increasing evidence suggests that the faulty trafficking of toxic amyloid proteins plays a crucial role in the disease pathology, primarily due to the alteration of their function (1).

The islet amyloid polypeptide (IAPP) or amylin is a 37 amino acid hormone synthesized and secreted together with insulin from the pancreatic islet β-cells (3, 4). IAPP is encoded by one single-copy gene in chromosome 12 (5, 6). Both proIAPP and proinsulin undergo similar posttranslational processing by prohormone convertases PC2 and PC1/3, as well as carboxypeptidase E (6). Fully processed IAPP is stored in secretory granules of pancreatic islet β-cells along with fully processed insulin. Upon physiological stimulation such as glucose increase in blood, insulin and IAPP are co-secreted at a molar ratio of 20:1 (7). Both hormones are implicated in glucose homeostasis (3, 4, 6). In addition to its physiological roles, studies also showed that human islet amyloid polypeptide (hIAPP) self-oligomerizes and aggregates in the pancreatic islets thereby inducing destruction of the islet β-cells, which in turn leads to insulin deficiency and type 2 diabetes mellitus (T2DM) (3, 4, 6, 8, 9). It is possible that similar to proinsulin (10–14), the deregulated trafficking of hIAPP could contribute towards β-cell failure during T2DM. Whereas many toxicity studies explored hIAPP aggregation mechanisms and its deleterious impact in T2DM, the mechanism and cellular factors regulating IAPP turnover in the pancreatic islet β-cells under normal and disease-relevant conditions are less clear.

Excessive intracellular and/or extracellular accumulation and aggregation of amyloid proteins has been increasingly recognized as the common pathological feature of amyloid diseases. Studies show nuclear accumulation of α-synuclein in the cultured cells, in α-synuclein-transgenic *Drosophila* and mice, and also in the human patients with clinically distinct synucleinopathy, suggesting its potential pathophysiological roles (1, 15). Similar to α-Synuclein, the intracellular domain of amyloid β precursor protein is transported to the nucleus suggesting its role in nuclear signaling (16). Previously, our lab demonstrated that synthetic hIAPP following internalization accumulates within the cytosol and nucleus of rat and human pancreatic islets (17). In agreement with α-synuclein studies, nuclear accumulation of extracellular synthetic hIAPP strongly correlated with its pathogenicity (17). However, possible nuclear accumulation of endogenous (native) hIAPP and its pathophysiological significance in respect to β-cell functions remains to be clarified.

Over the years there has been steady progress in understanding the impact of three hallmarks of T2DM: glucolipotoxicity, accompanying ER-stress, and islet amyloidosis on β–cell functions and viability (18–20). Typically, ER stress initiates cascades of signaling pathways collectively known as the unfolded protein response in an attempt to reduce the burden of cellular stress. Unfolded protein response activates cellular defensive mechanisms via three major signaling pathways, namely PERK, IRE1α, and ATF6 (20, 21). Independent studies have shown that chronic high glucose and associated ER stress alter insulin biosynthesis and secretion by regulating the expressions of the main insulin transcription factors PDX1 and MAFA (22, 23). In addition to glucolipotoxicity and ER stress, hIAPP was linked to β-cell stress and dysfunction leading to islet amyloidosis and T2DM in primates, including

humans, and transgenic animals (24–28). Despite similar gene structure and post-translation processing mechanisms, these two major glucose-regulating pancreatic hormones, insulin and IAPP differ significantly from each other with respect to their levels of gene and protein expressions and their responsiveness to glucose stimulus. For example, studies showed that in rat pancreatic islets the steady-state level of IAPP mRNA makes up to 10 fold less of the steady-state insulin mRNA (2). On the other hand, microarray and gene expression analysis revealed that hyperglycemia (24h) stimulated a ~10 fold increase in IAPP's mRNA where the insulin transcript levels remained unaltered (29). Based on these findings, it has been proposed that posttranscriptional modifications and differential promoter regulation could account for this differential expression of insulin and IAPP (30, 31). Studies showed that similar to the insulin promoter, the glucose regulation of the IAPP promoter is dependent on the binding of transcription factor PDX1 and also requires additional IAPP-specific transcription factors such as FoxA2 for its biosynthesis (31–34). Although both IAPP and insulin promoters share the ISL1 binding site as a common promoter element, the study demonstrates the involvement of ISL1 in the regulation of IAPP but not insulin promoter activity (34). Intriguingly, unlike insulin, IAPP promoter activity requires additional calcium responsive elements that are yet to be identified (32). A previous study has identified a thioredoxin-interacting protein (TXNIP) and IAPP as two major glucose upregulated genes (29). Independent studies demonstrated ER stress as one of the key upregulators of TXNIP (35, 36). Under physiological conditions, TXNIP regulates IAPP transcription by increasing the expression of transcription factor FoxA2 (31), whereas, insulin transcription is inhibited by TXNIP (37). Hence, differences in the IAPP and insulin transcription regulation could be accounted for at least in part by the involvement of the FoxA2 promoter element.

The current study demonstrates ER-stress associated FoxA2-dependent promoter activation, transcription, and accumulation of hIAPP in the biosynthetic compartments and the nucleus of insulinoma and human β-cells. Under ER stress, islet β-cells increased the rate of release of hIAPP, likely in an effort to reduce its excessive intracellular accumulation and possibly toxicity. In contrast to the proliferative action of insulin's c-peptide (38), the intracellular accumulation of hIAPP did not affect rRNA processing or proliferation of rat and human β-cells. Rather, intact nucleolar organization and functions were required for hIAPP production under normal and adverse conditions.

MATERIALS AND METHODS

Cell Culture and Treatments

For analysis of human (hIAPP) and rat (rIAPP) IAPP trafficking pathways, we created hIAPP- and rIAPP- stably expressing rat insulinoma (RIN-m5f) and insulin-secreting (INS 832/13) β-cells by transducing RIN-m5f or INS 832/13 cells with hIAPP-FLAG; rIAPP-FLAG or FLAG-tagged lentivirus particles (described below) followed by puromycin selection using a standard procedure (39). In some experiments, insulinoma cells transiently overexpressing hIAPP or rIAPP were used. RIN-m5f cells (ATCC, Gaithersburg, MD) and INS 832/13 parental line (a generous gift from Christopher Newgard lab at Duke University) overexpressing human or rat IAPP were cultured in RPMI 1640 medium (ATCC), supplemented with 10% (v/v) fetal bovine serum and 1% penicillin/streptomycin. HEK

293T cells (ATCC) were cultured in DMEM medium (Life Technologies) supplemented with 10% (v/v) fetal bovine serum and 1% penicillin/streptomycin. Cells were incubated at 37°C in a humidified incubator with 5% CO2 and passaged bi-weekly. Insulinoma cells (passage no. 15–40) were plated at a density of 50,000 cells per well and cultured for 12–16 hours prior to the experiments.

Human islets from diabetic and non-diabetic cadavers with >90% purity and viability were obtained through the Integrated Islet Distribution Program (IIDP) for Human Islet Research funded by the National Institute of Diabetes and Digestive and Kidney Diseases (NIDDK). The human islets that are distributed by the IIDP are from approved cadaveric organ and hence the tissue is exempt from human studies approval per IIDP guidelines. In the present study, the privacy and personal identity information of all participants were protected, i.e., all the data were analyzed anonymously. The study involving human islets was approved by the George Washington University Institutional Review Board (IBC# IBC-20-092). Upon arrival, islets were handpicked under a dissecting microscope to yield a purity of ≥ 95% (based on dithizone staining). Intact islets were suspended in CMRL media (ATCC) containing 1% (V/V) fetal bovine serum albumin and 1% penicillin/streptomycin and plated on 48-well non-adherent cell culture plastic plates at 30–40 islets per well for biochemical studies. Islets were cultured at 37 °C in a humidified incubator with 5% CO_2 for designated periods of time. For confocal studies, ~50–75 islets per well were gently dissociated in TrypLe cell dissociation medium (Invitrogen), plated on poly-D-Lysine coated 96-well glass-bottom black microplates (Thermo-Fisher), and allowed to adhere for 24h prior to treatments. To induce ER stress, cell cultures were treated with 0.5–1 μM thapsigargin (0–24h) or high glucose (20 mM) for an extended period of time (4 days). For small interfering RNA (siRNA) experiments, human islets (~500 IEQ per well/treatment) were incubated with 40 nM hIAPP-siRNA (Santa Cruz Biotechnology, cat# sc-39275) or scrambled siRNA control (Santa Cruz Biot.) for 5 hours, according to our previously established protocol (28). Transfections were performed in the presence of Lipofectamine 3000 (Thermo Fisher) in antibiotic-free islet media. Transfection media was replaced with regular islets culturing media, and incubations continued for an additional 48 hours. Following siRNA transfections, human islets cells were exposed to high glucose (20 mM) media for an additional 4 days, total RNA isolated and changes in gene expression levels analyzed with RT-qPCR.

Lentiviral particle production and lentivirus-mediated transduction

Flag-tagged ORF sequences for pre-pro-hIAPP and rIAPP, flanked with restriction enzyme sites (5’ SgfI and 3’ Mlu1) were synthesized using gBlock gene synthesis (Integrated DNA Technology) and cloned into a third-generation lentivirus destination vector (pLenti-C-Myc-DDK-IRES-Puro, Origene, cat# PS100069). Lenti-vpack packaging kit containing lentivirus packaging plasmids were obtained from Origene (cat# TR30022). Lentivirus particles were generated following the lentivirus packaging protocol provided by Origene. Briefly, HEK 293T cells were plated in 75cm^2 flasks in a cell density of 300,0000 using a normal growth medium and incubated at 37°C overnight. Cell transfection was carried out with 5μg of the lenti-ORF (hIAPP/rIAPP) expression construct and 6μg of lentivirus packaging plasmids using MegaTran transfection reagent (Origene, cat# TR30022). After 12–18 hours of incubation, the transfection mixture was replaced with a normal growth medium. A first and

second batch of viral supernatant was harvested at 24 h and 48 h intervals respectively, combined, spun at 3000 rpm/min, and filtered through a 0.45-micron filter to remove cellular debris. Lentivirus particles were concentrated using the Lenti-X™ Concentrator (Clontech, cat# 631231) and stored at −80°C. Lentivirus titer was calculated using ELISA-based Lenti-X™ p24 Rapid Titer Kit (Clontech, cat# 632200) following the manufacturer's protocol. Lentivirus-mediated hIAPP and rIAPP overexpression were carried out with RIN-m5f cells. Briefly, RIN-m5f cells at the density of 50,000 cells per well or partially dispersed human islet cells were plated in 12 well tissue culture plates. After 24 hours of cell plating, lentivirus particles encoding hIAPP or rIAPP were added at the MOI (multiplicity of infection) of 300 and incubated for 5 hours. Polybrene (1000X stock, 8mg/ml) was used during the transduction procedure to ensure efficient viral integration. Lenti virus-containing medium was replaced with normal growth medium and the cells were allowed to grow for an additional 48 hours at 37°C. Cells were then used for downstream analysis.

Cell fractionation

Human islets were incubated in 5mM or 20mM glucose-containing media for 4 days. Media was removed, cells washed with PBS, and briefly incubated for 5 min at +4°C with a set of membrane-permeabilizing detergents provided in a cell fractionation kit (Invitrogen, cat# 78840) according to the manufacturer's protocol. Using this approach, four distinct subcellular fractions were isolated: cytoplasmic, ER/Golgi, nuclear soluble, and chromatin-enriched fraction. The purity of fractions was confirmed with western blot using specific antibodies against organelle markers.

Western blot analysis

Intracellular content of hIAPP in human islets and transfected RIN-m5F cells were determined by western blot. Whole-cell lysates from the lentivirus transduced RIN-m5f cells or human islets were collected using RIPA buffer (EMD Millipore, cat# 20-188) supplemented with protease (Life Technologies, Inc, cat# 1862209) and phosphatase inhibitor (Life Technologies, Inc, cat# 1862495) cocktails. Protein concentrations in each of the whole cell lysate samples were analyzed using BCA assay (Thermo Fisher, cat# 23228). Conditioned media (500μl) were collected from each experimental group and residual cells were removed by centrifugation. Equal protein content (10 μg) of whole-cell lysates or cellular fractions and equal volumes (15 μl) of conditioned media were loaded on a 4–15% Tris-Glycine SDS PAGE and proteins separated under reducing conditions. Resolved proteins were transferred to nitrocellulose membranes (Bio-Rad) and non-specific IgG binding sites were blocked by incubation with 5% nonfat dry milk (VWR). Membranes were probed with primary antibodies at 4°C overnight, followed by the addition of corresponding horseradish peroxidase-conjugated secondary antibodies at 1:2000 dilutions (Thermo Fisher) for 1 hour at room temperature. Following primary antibodies were used: rabbit anti-FLAG antibody (1:500, Novus Biologicals, cat # NB600-345), cytoplasmic fraction marker-mouse HSP90 (1:200, Santa Cruz Biotechnology, cat # sc-101494), secretory vesicle marker-rabbit VAMP 1/2/3 (1:200, Santa Cruz Biotechnology, cat# 133129.), endoplasmic reticulum marker-rabbit calnexin (1:1000, Abcam, cat# ab22595), Golgi marker-rabbit GM130 (1:1000, Abcam cat# ab52649), nuclear soluble fraction marker-rabbit histone deacetylase 2 (HDAC2, 1:1000, Abcam, cat# ab16032), chromatin-bound fraction marker-rabbit histone

(1:1000, Abcam cat# ab1791), mouse IAPP (1:200, Santa Cruz Biotechnology cat# sc-377530), rabbit insulin (1:1000, Abcam cat# ab181547). Blots were developed using a pico ECL substrate kit (Thermo Fisher, cat# 32209) and documented using the BIO-RAD gel imaging station. Band's intensity, reflecting relative protein expression, was determined with a Bio-Rad Image-Lab software. Actin was used as the loading control. The relative protein content in cellular fractions was calculated and expressed as the percentage of the total protein load/expression in a given blot. The data (% protein content) was derived from three separate sets of experiments and averaged.

Immunocytochemistry

For alkaline phosphatase assay, control and hIAPP/rIAPP-transfected RIN-m5f cells were washed in PBS (3x) and fixed with acetone for 20 minutes at −20°C. IAPP expression was detected by incubating the cells with rabbit polyclonal anti-FLAG antibody (1:200, Novus Biologicals, cat # NB600-345) at room temperature (RT) for 2 h followed by goat anti-rabbit alkaline phosphatase-conjugated secondary antibodies (1:500, Abcam, cat# ab97048) for 60 minutes at RT. Following this, cells were washed with PBS (3x) and incubated with 1-Step NBT/BCIP plus suppressor (Thermo Scientific, cat# 34070) for ~10 min. Cells were washed with ddH20 and images captured using a light microscope (Motic) and 10x objective.

For immuno-confocal microscopy, following treatments, cultured RIN-m5f or partially dissociated human islet cells were washed in PBS (3X) and fixed with 4% paraformaldehyde for 20 minutes. Following fixation, several blocking steps were performed. First, cells were incubated with *Image IT* solution from Fisher (cat # I36933) at RT for 30. min to reduce background and non-specific interactions in subsequent immuno-staining steps. Cells were then washed 3x in PBS and incubated in 3% bovine serum albumin (BSA) / PBS solution for 1h at room temp as a second blocking step. We also included this blocking agent (1% BSA) in all our incubations with primary and secondary antibodies. Omissions of primary or secondary antibodies produced a negligible (autofluorescence) signal below a threshold used to generate immune-confocal images. Following blocking steps, cells were permeabilized using 1% BSA/0.1 % Triton X-100 PBS solution for 30 min. at 4°C. IAPP accumulation was then detected by incubating the cells with mouse monoclonal anti-IAPP antibody (1:200, Santa Cruz Biotechnology, cat # sc-377530) at 4°C overnight followed by goat anti-mouse Alexa 647-conjugated secondary antibodies (1:500, Invitrogen, cat# A21236) for 60 minutes at RT. Cells were further incubated with specific organelle marker antibodies or rabbit polyclonal anti-insulin antibody (1:500, Abcam, cat# ab181547) and anti-rabbit Alexa 488-conjugated secondary antibodies (1:500, Invitrogen, cat# A21441), each for additional 60 minutes at RT. Nuclei were stained with nuclear-specific dye, DAPI (Cell Signaling Technology, cat# 4083) for 10 min at RT. The following antibodies (Abcam) were used: ER marker, anti-calnexin (1 : 500, cat# ab22595); Golgi marker, anti-GM130 (1 : 500, cat# ab52649); and nucleolar marker, anti-nucleolin (1 : 200 cat# ab22758). For the detection of proliferating cells, partially dispersed human islet cells were stained with anti-Ki67 antibody (1:500, Abcam, cat# ab16667). For the detection of aggregated proteins, paraformaldehyde-fixed T2DM human islets were incubated with Thioflavin-T (Th-T) (Sigma, cat# 596200) staining solution (0.5% Th-T in 0.1N HCl) for 10 mins at RT. The non-bound Th-T stain was removed by washing cells with 0.1M HCl in PBS for 1 min.

Three random fields in each well were imaged by confocal microscopy and the Z-series (Z-1 μm for RINm5f cells and Z-5μm for human islets) optical sections were acquired for each field using a ZEISS LSCM-800 confocal microscope (Carl Zeiss, Thornwood, NY) and 63X (1.3 N.A.) or 100X oil objective. The pinhole was adjusted to keep the same size of Z-optical sections for all channels used. Multitrack imaging was performed to ensure that there was no crosstalk between the channels. The range indicator and the Zeiss intensity analysis platform were used to remove any saturated pixels from fluorescence images. Colocalization analysis was performed on a pixel-by-pixel basis using ZEN software from Zeiss. The intensity thresholds of the channels were set using the Zeiss cross-hair function and single label control samples were imaged with the same acquisition (laser power and PMT) settings to avoid setting an arbitrary background threshold. In that way, the background pixels that might contribute to false colocalization were excluded from the analysis. The Pearson correlation coefficient (R) was determined using Zeiss co-localization software (ZEN Blue). Obtained R-values were averaged and grouped in four categories: no colocalization $R< 0.1$ low colocalization, R=0.1–0.3, partial colocalization R = 0.3–0.6 and high co-localization $R > 0.6$. Original images were exported and assembled using Adobe Photoshop software (Adobe Systems). Quantification of fluorescence intensity signals in micrographs, reflecting relative protein expression levels, was performed with Image J. Two to three random fields from each well (experimental group) were imaged by confocal microscopy. Multiple (6–10) optical sections (5 μm Z-axis) from top to bottom of the islets were acquired for each field (control and treatments). hIAPP fluorescence signal (intensity) in each cell was then determined using a freehand area selection tool in Image J, and data averaged. Between 50 and 75 cells from each experimental group (n=2), were used for quantitative analysis. Imaris and Arivis microscopy software were used for 3D-analysis of protein (hIAPP) distribution within Z-stack optical sections (movies S1 and S2).

Transmission Electron Microscopy

hIAPP-overexpressing and control (rIAPP-expressing) INS 832/13 cells (~ 50×10^3) were washed twice in PBS, pelleted in a microcentrifuge, and fixed with 2% PFA and 0.5% glutaraldehyde in 0.1 M sodium cacodylate buffer for 60 min on RT. Cells were embedded in agarose and dehydrated before infiltration with LR White resin. Then ultrathin sections were cut with a diamond knife on an ultramicrotome. Sections were placed on formvar, carbon-coated nickel grids, and exposed to blocking solution (5% Normal Goat Serum in 20 mM Tris buffer, 0.15 M NaCl, 0.1% BSA) and incubated with primary anti-human hIAPP antibody (1:50, Santa Cruz) diluted in 20 mM Tris buffer, 0.15 M NaCl, 0.1% BSA overnight at room temperature. Sections were washed and incubated with secondary anti-mouse 10 nm gold conjugated particle (Sigma) at 1:40 dilution with 20 mM Tris buffer, 0.15 M NaCl, 0.1% BSA for 1hr. Sections were washed, fixed with 1% glutaraldehyde, and stained with 1% uranium acetate and lead citrate before imaging. Images were acquired with the FEI Talos F200X transmission electron microscope (ThermoFisher) at 80 kV with a CETA 16M camera. SEM micrographs were then imported into Image J for analysis of IAPP particle distribution. Data represent an averaged number (mean ± SEM) of IAPP's immuno-positive gold particles in 5 to 7 randomly chosen cross-sectional areas of the nucleus or cytoplasm of each cell. Between ~60 and 75 cells were used for quantitative analysis.

Cell Proliferation Assay

β-cell proliferation in cultured human islets was evaluated using two independent cell proliferation assays: an EDU incorporation assay followed by immunostaining and double Ki67/hIAPP immunostaining. EdU (5-ethynyl-2′-deoxyuridine) is a nucleoside analog of thymidine and is incorporated into newly synthesized DNA (40). Ki67 is a nuclear protein and has been widely used as a marker for cell proliferation (41). The nuclear antigen of Ki67 is expressed in biosynthetic phases of the cell cycle such as S, G1, and M but absent during the G0 phase (42, 43). EDU incorporation is a cell proliferation identification based on new DNA synthesis. Non-diabetic human islets were cultured in basal (5mM) or high glucose (20mM) media for 4 days to stimulate cell proliferation and hIAPP production. Click-iT EDU assay was performed using the Click-iT EDU imaging kit (Life Technologies, cat # C10637) according to the manufacturer's instruction. EDU incorporation assay was followed with immuno-probing of hIAPP. For Ki67 staining, human islets were fixed, permeabilized, and immunostained with Ki67 and hIAPP antibodies using the ICC approach described above. Three to five random fields in each well were imaged by confocal microscopy and multiple optical sections (5μm Z-axis) from top to bottom portion of the cells were acquired for each field. Three to six optical sections covering the top, middle, and bottom of each image with three images per sample (control and treatment) were analyzed. The proliferation rates of hIAPP-expressing islet cells under normal and HG conditions were calculated by double-counting nuclear hIAPP and EDU (or nuclear Ki67) positive and negative cells within the field. On average, 10 to 50 hIAPP positive cells were counted in each optical field, with 3 random fields analyzed per experimental group (performed in triplicates).

Quantitative real-time PCR (qRT-PCR) analysis

Total RNA was extracted from INS 832/13 cells or human islets using TRIzol reagent (catalog no. 15596026, Life Technologies, Inc.) and the RNeasy mini kit (catalog no. 74134, Qiagen) according to the manufacturers' instructions. Total RNA was further purified from contaminating DNA using in-column DNA digestion with RNase-free DNase, following the manufacturer's instructions (catalog no. 79254, Qiagen). cDNA was synthesized from 500 ng of RNA using multiScribeTM reverse transcriptase and random primers (High Capacity cDNA Reverse Transcription kit, catalog no. 4368814, Applied Biosystem) according to the manufacturers' protocol. qPCR was performed using the Bio-Rad CFX 96 real-time system (C1000 Touch thermal cycler). Briefly, relative gene levels were detected in the reverse-transcribed cDNA using iTaqTM Universal SYBR Green supermix (catalog no. 1725122, Bio-Rad) using the following thermal cycling protocol: polymerase activation 95 °C, 2 min; DNA denaturation 95 °C, 5 s; annealing and extension 60 °C, 30 s; repeat 40 cycles. All RT-qPCR primer sets are presented in Table S1. Gene expression levels were normalized to actin expression. Relative mRNA levels were calculated using the $2^{-\Delta CT}$ method (51).

Promoter Activity Assay

IAPP promoter activity assay was performed using our previously published protocol (44). Briefly, the total genomic DNA of HEK293T cell was purified using Qiagen Core Kit (Qiagen, cat# 201223). The full hIAPP promoter region was amplified (from 2000bp upstream of the transcription start site to the first exon) using hIAPP gene-specific primers

(Table S1) and the KOD hot start PCR kit, following manufacturer's instruction (EMD Millipore, cat# 71842). The isolated promoter was purified using the QIAquick gel extraction kit (Qiagen, cat# 28704) and ligated into the PCR-Blunt II-TOPO vector (Life Technologies, cat# K280020). Isolated clones were confirmed by Sanger sequencing (GENEWIZ). Selected clones were then sub-cloned into a firefly luciferase encoding pGL3 basic vector (a gift from Richard Day, Indiana University) using BgIII and NcoI restriction sites, thus generating the hIAPP promoter-firefly luciferase construct. In addition to this wild-type-hIAPP promoter, the hIAPP-ΔFoxA2-Luc promoter construct was generated using the Q5® Site-Directed Mutagenesis Kit (New England Biolabs, Cat# E0554S) following the manufacturer's instructions. The hIAPP-ΔFoxA2-Luc promoter has a single base substitution (TTTA>TGTA) in the proximal conserved FoxA2 binding site (Fig. 8B). The primer set used for site-directed mutagenesis is presented in Table S1. The sequence of the hIAPP-ΔFoxA2-Luc was verified using sanger sequencing. For transfection, either dispersed human islets or RIN-m5f cells were plated on 96-well tissue culture plates using FBS and penicillin/ streptomycin free growth media (as described before). Following 16–24 h of plating, cells were co-transfected with PGL3 basic (empty vector control) or hIAPP-Luc or hIAPP-ΔFoxA2-Luc and Tk Renilla promoter vector (gift from Richard Day, Indiana University) using Fugene HD (Promega, cat# E2311) transfection reagent. Transfected human islets or RINm5f cells were cultured for an additional 48 h and treated with either vehicle control (DMSO) or thapsigargin (0.5μM) for the final 24h or high glucose (20mM) for the final 48h. Luciferase activity was detected using the Dual-Glo Luciferase Assay System (Promega, E2920) following the manufacturer's instructions. Transfection efficiency was normalized by the Tk Renilla promoter activity.

Statistical Analysis

The Graph Pad Prism 7 Program was used for plotting and statistical analysis. The unpaired Student's t-test or one-way ANOVA followed by the Tukey post-hoc test was used for pairwise comparisons among groups when appropriate with significance established at $p < 0.05$. The number of independent biological replicates per treatment group is listed in the figure legend.

RESULTS

IAPP follows bipartite trafficking routes in β-cells

To study IAPP trafficking, we transiently overexpressed the FLAG-tagged human (hIAPP-FLAG) and rat (rIAPP-FLAG) pro-IAPP forms in pancreatic rat insulinoma RIN-m5F cell line using lentivirus-mediated gene delivery method. This rodent pancreatic β-cell line produces small amounts of endogenous rat IAPP (rIAPP), which makes RIN cells particularly suitable for hIAPP overexpression and trafficking studies. Immunocytochemistry analysis revealed high (≥60%) transduction efficiencies for hIAPP and rIAPP constructs in these cells (Fig. S1A). Consistent with this result, western blot analysis revealed a marked increase in protein expression levels of hIAPP and rIAPP in the RIN-m5f cell within 48h of transduction (Fig. S1B). ELISA assay confirmed a significant increase of IAPP isoforms in transfected cells (data not shown). This noticeable

accumulation of hIAPP in the conditioned media of hIAPP-expressing RIN-m5f cells indicated proper vesicular transport and secretion of the overexpressed hIAPP (Fig. S1C).

Intracellular trafficking pathways of hIAPP were examined by confocal microscopy (Fig. 1A, B). To distinguish human from rat IAPP in these immunocytochemistry studies we used an anti-IAPP monoclonal antibody that has a higher affinity towards human isoform (Figs. 1–2, Fig. S1). Fluorescent confocal microscopy revealed a strong expression of hIAPP in hIAPP-transduced but not in control (EV-transduced) RIN-m5f cells (Fig. 1A). 3-D confocal microscopy analysis showed a strong hIAPP signal in cytosolic/perinuclear regions of transfected cells as well as numerous hIAPP-positive fluorescence puncta (arrows) within the nuclei of these cells (Fig. 1B; Fig. S2). To resolve whether hIAPP nuclear accumulation is a specific and transient trait of RIN-m5f cells, we implemented a high-resolution EM approach to examine IAPP trafficking pathways in another rat β-cell line, INS 832/13, that stably overexpress hIAPP. Using TEM and gold tagged anti-IAPP monoclonal antibodies, we detected a small number of rat IAPP positive immunogold particles in the cytoplasm and nucleus of control cells (Fig. 2A, B). In line with cell fractionation and microscopy studies in RIN-m5f cells, the high-resolution immuno-EM analysis revealed the extracellular (Fig. 2 C, D) and intracellular accumulation of hIAPP immune-gold particles in the nuclei and perinuclear regions (Fig. 2E, F) of hIAPP-expressing INS 832/13 cells indicating their proper processing and vesicular transport/secretion in these cells. Interestingly, IAPP-positive gold particles were also observed in mitochondria and autolytic compartments (Fig. 2G, H), in agreement with previous reports (17, 45–48). In accord with confocal microscopy, there was a significant (3–4 folds) increase in IAPP signal in cytoplasmic and nuclear regions of hIAPP-expressing stable cells as compared to control INS 832/13 cells expressing native rat IAPP (Fig. 2I, J), demonstrating the tendency of both IAPP isoforms to accumulate in these two major cellular compartments.

High glucose differently affects hIAPP and insulin trafficking in primary human islet cells

Next, we sought to resolve IAPP and insulin trafficking pathways in primary human islet cells and the impact of cellular stress on their routing in cells. Freshly isolated human islets procured from non-diabetic individuals were cultured under normal 5mM glucose (Glc) or glucotoxic conditions (by exposing islets to 20mM glucose (Glc) media for 4 days). Following incubations, subcellular fractions were prepared using a cell fractionation approach followed by western blot analysis. Western blot confirmed isolation of four enriched subcellular fractions, namely cytoplasmic (CT), Golgi/ER-enriched organelles (OR), soluble (NS), and chromatin-containing (NC) nuclear fractions as evident from the redistribution of organelle/compartment-specific markers, HSP90, calnexin, HDAC2, and histone, respectively (Fig. 3A). The CT fraction was enriched in secretory vesicles and soluble cytoplasmic proteins as it contained a major intracellular pool (≥ 95%) of vesicle specific marker, VAMP, and HSP-90 (Fig. 3A). We also detected a relatively minor (≤ 20%) contamination of cytosolic fraction with organelle and nuclear fractions (but not vice versa, Fig. 3A). The organelle (OR) fraction contained 75% of ER marker calnexin relative to other subcellular fractions (Fig. 3A). Importantly, the OR fraction was depleted of cytosolic (HSP90) and secretory vesicles (VAMP) proteins (Fig. 3A). It contained a minor nuclear component based on H3 staining. However, less than 10% of H3 intracellular content was

found in extranuclear compartments (Fig. 3A). Finally, nuclear fractions were highly enriched in nuclear marker protein, histone (>90%) compared to other subcellular (cytosolic/secretory/biosynthetic) fractions with traces (≤ 2%) of contaminations coming from these three fractions (Fig. 3A). Western blot analysis showed that each fraction sequestered at least 75% of the total intracellular content of compartment's/organelle's-specific markers, thus demonstrating an efficient separation between fractions.

It is well established that high glucose stimulates hIAPP biosynthesis in pancreatic β-cells (2, 29–31). Consistent with this fact human islets cultured under these stimulatory conditions (20mM Glc for 4 days), showed elevated hIAPP intracellular levels in all three subcellular fractions as compared to control islets (cultured in 5mM Glc media) (Fig. 3A–D). Western blot revealed the significant accumulation of hIAPP (~40% of the total intracellular hIAPP pool) in the cytosolic VAMP-positive (CT) fraction of human islet under basal (5mM Glc) conditions (Fig. 3A, E). The remaining hIAPP was distributed between Golgi/ER-enriched fraction and the nucleus (Fig. 3A, E). A similar distribution pattern was observed in high glucose (20mM Glc) treated human islets (Fig. 3F). In contrast to hIAPP, insulin was not found in detectable levels in the nucleus in either condition (Fig. 3A).

High glucose and ER stress stimulate trafficking of monomeric hIAPP to nuclei of pancreatic β-cells

Here we investigated how elevated blood glucose levels and ER stress affect the intracellular turnover of hIAPP, as they are both major and interrelated attributes of T2DM. To this end, we used the potent and selective ER-stress agent, thapsigargin (0.5 μM, 24 h) and media supplemented with high glucose (20mM Glc, for 4 days). High glucose (20mM Glc) treatment induced ER stress in cultured human islets as reflected by a marked increase in ER stress marker, BIP (Fig. 4A). Co-staining of islets with insulin and hIAPP specific antibodies showed a partial co-localization of these two β-cell hormones in the cytoplasmic and perinuclear regions (denoted by arrowheads) of control non-diabetic islets, ($R=0.59 \pm 0.03$, $n=3$, Fig. 4B, scatterplot), reflecting their co-synthesis and co-transport under normal physiological conditions. Interestingly, decreased cytosolic and increased nuclear hIAPP accumulation (denoted by arrows) was detected in islet β-cells procured from confirmed T2DM patients with a long (≥ 10 years) history of the disease (Fig. 4B). This decrease in hIAPP cytosolic signal in diabetic islets is consistent with a loss in hIAPP transcripts (mRNA) and protein levels that has been previously reported in these patients (44). In agreement with T2DM studies, confocal microscopy revealed a significant ~ 40% increase in the number of nuclear hIAPP positive β-cells in high glucose- and thapsigargin-treated cells as compared to control non-diabetic islets (Fig. 4C, D). The only difference in hIAPP turnover between these two model systems was observed in the cytoplasm: short-term stress evoked by high glucose and thapsigargin stimulated hIAPP accumulation in the cytoplasm of freshly isolated cultured islet β-cells (Fig. 4C, arrowheads). The cytoplasmic accumulation of hIAPP can be attributed, at least in part, to stimulatory action of high glucose on hIAPP biosynthesis (Fig. 3). The findings from our *ex vivo* studies mirror clinical studies showing two distinct phases in IAPP turnover: hyperamylinemia, during early stages of diabetes, followed by decreased hIAPP production or hypoamylinemia during the late-onset of the disease (49).

We also examined the molecular form(s) of nuclear hIAPP by co-staining T2DM human islets with hIAPP specific antibody and amyloid-specific stain Thioflavin-T (Th-T). Immuno-confocal microscopy revealed small clusters ($d \leq 1\ \mu m^2$) of perinuclear/cytosolic Th-T- and hIAPP-positive structures, indicating the accumulation of protein, and possibly hIAPP, aggregates (Fig. S3A, arrowheads). However, colocalization analysis (Fig. S3A, scatterplot) revealed that hIAPP was not an integral component of these cytosolic Th-T positive structures as a very low co-localization value was obtained between these two assemblies in T2DM islet cells ($R^2=0.15 \pm 0.08$, n=3). hIAPP (arrows) was again detected in the nuclei of islets β-cells procured from another T2DM donor (Fig. S3A, inset). Western blot analysis revealed the presence of monomeric but not oligomeric hIAPP in the nuclear compartments of non-diabetic control and high-glucose (HG) treated islets (Fig. S3B). Collectively, this data demonstrates the increased accumulation of a soluble, monomeric, and mature form of hIAPP in the nuclei of human β-cells following induction of cellular stress. The high-resolution 3-D confocal analysis confirmed the nucleus as an important accumulation site for intracellular hIAPP and even suggested possible hIAPP association with the nucleolus as conspicuous hIAPP-positive nucleolar structures were detected in cultured human islet cells (Fig. 5A, movies S1 and S2). The nucleolar localization of hIAPP in human islets was indeed confirmed by indirect immunocytochemistry showing co-staining of hIAPP with nucleolar marker proteins, nucleolin (Fig. 5B), and TIA-1 (Fig. S4). Confocal microscopy further revealed the significant (~ 25%, 50%, and 70%) increase in mean hIAPP fluorescent intensity signal within the nucleolus of high glucose treated (20mM, 4 days), thapsigargin treated (0.5μM, 24 h), or in confirmed T2DM islets as compared to control islets cultured in 5mM Glc, respectively (Fig. 5B, C).

hIAPP expression and nuclear accumulation does not affect β–cell proliferation nor ribosomal RNA synthesis

The fact that hIAPP regularly accumulates in the nucleolus and other nuclear regions such as chromatin under normal and diabetes relevant (HG, ER stress) conditions (Figs. 3–5) raises a question about the functional significance of hIAPP's transport and accumulation in the nucleus. The nucleolus is the dynamic nuclear compartment involved in ribosomal biosynthesis, which is the rate-limiting step in protein syntheses and thus cell proliferation (50, 51). Based on this fact, we inquired here if the expression and nuclear accumulation of hIAPP affect β-cell proliferation. The turnover of hIAPP and human islet cells under basal and high glucose conditions was investigated using two independent proliferation assays: EDU incorporation and Ki67 staining. A high glucose (20mM) treatment markedly increased nuclear localization of hIAPP (~90% of total hIAPP positive cells) as compared to islets cultured in basal 5mM Glc (~60% of total hIAPP positive cells) (Fig. 6A, B). Confocal microscopy revealed a modest but significant increase (~20%) in the number of proliferative (EDU-positive) islet cells in high glucose media (20mM) as compared to control human islet cells (5mM Glc) (Fig. 6A, C). Interestingly, confocal microscopy experiments showed a disproportionally smaller number of nuclear $hIAPP^+$ / EDU^+ double-positive cells (~20%) and a larger number (~80%) of nuclear $hIAPP^+/EDU^-$ human islet cells following exposure to HG (Fig. 6A, C). Ki67 staining showed a similar 4-fold difference between nuclear $hIAPP^+/Ki67^+$double positive cells (~20%) and non-proliferative $hIAPP^+/Ki67^-$ (~80%) islet cells under the same conditions (data not shown).

Previously, the nucleolar accumulation of insulin processing fragment, C-peptide, was linked to rRNA synthesis and cell proliferation (38). Like C-peptide, hIAPP accumulates together with nucleolin and TIA1 in the fibrillary region of the nucleolus (Fig. 5A, B; Fig. S4). Therefore, we examined the potential role and impact of ectopic and HG-induced hIAPP gene expression on 18S and 47S ribosomal precursor gene transcription using a qRT-PCR approach (Fig. 6D, E). We used this sensitive quantitative method because of its high dynamic range and ability to simultaneously detect changes in biosynthetic rates for the abundant and scarce transcripts such as rRNA and mRNA of ribosomal subunits and hIAPP, respectively. High glucose (20mM) stimulated a significant (~3-fold) increase in relative hIAPP mRNA levels as compared to human islets cultured under normal 5mM Glc conditions (Fig. 6D). Expectedly, glucose-responsive genes, TXNIP, and Ki-67 were also significantly upregulated by this treatment (Fig. 6E). Using an RNAi approach, we were able to specifically and markedly (≥ 2.5-fold) downregulate cellular levels of hIAPP mRNA transcripts relative to HG and scrambled oligos (HG/RNAsc)-treated cells (Fig. 6D). However, hIAPP gene silencing had no significant effect on gene expressions of insulin (Fig. 6D), a mature 18S (data not shown), or its precursor (47S) rRNA (Fig. 6E). Similarly, lentivirus-mediated overexpression of hIAPP in human islets did not have any significant modulatory effect on 47S rRNA levels (Chatterjee Bhowmick and Jeremic, unpublished observation). Expression of the proliferative marker, Ki-67, was also not significantly affected by hIAPP knockdown, either under normal or HG conditions (Fig. 6E). Thus, hIAPP expression and nuclear accumulation are not required for ribosomal subunits synthesis under normal or HG conditions.

IAPP biosynthesis is increased in ER-stressed human islet cells

Prolonged HG treatment induced concurrent ER stress and hIAPP synthesis in human islet β-cells (Figs. 3, 4, 6) suggesting mechanistic and possible functional connections between them. To confirm a causal link between ER stress and hIAPP turnover in β-cells, freshly isolated, cultured human islets were treated with increasing concentrations of the selective ER stress inducer, thapsigargin (TG, 0.5μM) for 24 h and hIAPP transcript and protein levels analyzed with qPCR and western blot, respectively (Fig. 7). Western blot analysis of the human islet extracts revealed increased levels (≥ 2.5 folds respective to vehicle) of ER stress marker chaperon protein GRP78/Bip following TG treatment, confirming induction of ER stress (Fig. 7A, B). Similarly, a significant rise in hIAPP protein levels (~2 folds increase) and to a lesser extent insulin protein levels (~1.5 fold) with the addition of thapsigargin was observed (Fig. 7A, C, D). It was reported that ER stress may disturb secretory pathways and disrupt the integrity of the Ca^{2+}-signaling complexes in many cells including pancreatic β-cells (52, 53). Thus, ER stress may increase intracellular hIAPP levels by impeding the processing and/or secretion of this hormone. To test this scenario, we analyzed the levels of extracellular hIAPP before and after ER stress induction. Contrary to this idea, western blot analysis of the conditioned media from human islet cells showed increased extracellular levels of fully processed hIAPP following induction of ER stress with 0.5 μM thapsigargin (Fig. 7A). In agreement with our protein studies, gene expression studies using qPCR demonstrated a moderate but significant increase in transcription of hIAPP (~2.5 fold) and to smaller extent insulin (~1.5 fold) genes following induction of ER stress (0.5μM TG, 24 h, Fig. 7E).

An intact nucleolar organization and function are required for hIAPP production under normal and ER stress conditions

To fully clarify a causal link between hIAPP turnover, nucleolar organization, and ER stress, we examined hIAPP production in normal and ER-stressed human islets featuring normal and compromised nucleolar structure/function. To this end, we used RNA Pol II inhibitor, α-amanitin, in concentrations that were previously shown to disrupt nucleolar organization and function in cells (54). Nucleolar marker and regulator of ribosomal synthesis, nucleolin, was expressed in all control islet cells and localized to both nucleoplasm and nucleolus (Fig. S5A). Following induction of ER stress with thapsigargin (TG, 0.5 μM, 24h), IAPP and nucleolin signal increased by 1.9 and 3.1-fold respectively, reflecting its upregulation in human islet cells under these conditions (Fig. S5B, E). Like the RNA Pol I inhibitors (55), RNA Pol II inhibitor, α-amanitin, disrupted nucleolar organization in human islet cells as shown by loss of nucleolin puncta in the nucleolus and its diffuse redistribution across the nucleoplasm. This disruptive effect of α-amanitin on nucleolar organizations was noticeable in both control (Fig. S5C) and TG-treated cells (Fig. S5D). Importantly, this loss of nucleolar organization and inhibition of RNA Pol II activity by α-amanitin markedly (> 70%) suppressed hIAPP and to a lesser extent nucleolin expression in both control and ER-stressed human islet cells (Fig. S5C, E). We also observed a marked suppressing effect of α-amanitin on HG-induced hIAPP protein expression in human islets (data not shown). Thus, intact nucleolar organization is critically important for hIAPP synthesis under normal and adverse conditions, but not *vice versa*.

FoxA2 is required for ER stress-induced hIAPP transcription in rat and human islet cells

Next, we used promoter activity assay (Fig. 8) to determine the mechanism and role of IAPP's critical transcriptional factor, FoxA2, in ER stress-induced hIAPP transcription in β-cells. Within three FoxA2 binding sites, the proximal FoxA2 site (with respect to the transcription start site, Fig. 8A) plays a critical role in the glucose-induced expression of IAPP (31). Hence, by using the full (wild type) and single mutant hIAPP-ΔFoxA2 promoter constructs (Fig. 8B), we tested here if functional FoxA2 binding sites are also required for hIAPP synthesis under ER stress conditions. Following induction of ER stress (0.5μM TG, 24h), promoter activity assay revealed a significant and marked increase in luminescence signal (>2 fold) in constructs driven by wild-type-hIAPP promoter both in primary human islets and RIN-m5f cells (Fig. 8C, D). In line with the previous reports (31), the functional null hIAPP-ΔFoxA2 promoter was significantly less active under both basal (5mM Glc, a 40% decrease), high glucose (20mM Glc, a 90% decrease), and ER stress (0.5μM TG, a 50% decrease) conditions compared to the wild type-hIAPP promoter (Fig. S6; Fig. 8C, D). Interestingly, in spite of its stimulatory action on insulin transcription (Fig. 7E), ER stress induced by 0.5μM TG (24h) failed to significantly alter insulin promoter activity (Fig. 8E), suggesting a post-promoter regulation of insulin transcription under these conditions.

Gene expression of FoxA2-regulatory protein TXNIP is upregulated in ER-stressed human islets and correlates with hIAPP transcription

Thioredoxin-interacting protein (TXNIP) was previously implicated in FoxA2-mediated IAPP gene expression in rat and human β-cells cultured under normal and high glucose

conditions (31). This study demonstrated that overexpression of TXNIP increases IAPP transcription by promoting FoxA2 enrichment at the proximal FoxA2 binding site in the IAPP promoter (31). Interestingly, TXNIP is a common target of both ER stress and metabolic (glucose) pathways in islets and other cells (36, 56, 57). Thus, it is conceivable that ER stress and high glucose conditions associated with T2DM may upregulate hIAPP transcription via shared TXNIP-mediated signaling. To attest this, we performed comparative transcriptomic analysis of hIAPP, insulin, and TXNIP gene expression in ER-stressed and high glucose challenged human islets (Fig. 9). The use of selective ER-stress agents, thapsigargin (TG) and tunicamycin (TN) are advantageous to separate metabolic and stress effects on gene expression. Compared to control islets, the qPCR analysis revealed a significant (1.9±0.4, 2.7±0.5 and 3.4±0.3 folds) increase in hIAPP mRNA levels by TG, TN, and HG treatments, respectively (Fig. 9). By contrast, insulin mRNA levels remained comparable (1.1–1.3 folds) to controls in all treatments (Fig. 9). hIAPP gene expression strongly correlated with the expression pattern of TXNIP evoked by these three agents. HG was the most effective in inducing TXNIP expression (8±0.3 fold) vs 1.7±0.4 and 2.6±0.2 folds for TG and TN, respectively (Fig. 9). Expectedly, synthetic ER-stress inducers were more potent in inducing ER stress as compared to HG treatment, reflected by an additional 2–3-fold increase in levels of ER-stress marker BIP in TG- and TN-treated cells (3.9±0.4 and 8.9±0.9 folds) as compared to HG-exposed islets (1.6±0.3 fold, Fig. 9). Although overexpression of TXNIP may significantly elevate FoxA2 transcript and protein levels (31), we observed a small and non-significant increase of FoxA2 and PDX1 mRNA levels in stressed (HG/TG/TN-treated) β-cells respective to controls (1–1.4 folds, Fig. 9). Even though metabolic (HG-induced) pathways appear to be more potent in activating the TXNIP signaling pathway and its downstream targets such as hIAPP than the synthetic ER-stress inducers, it is important to note that the TXNIP/FoxA2-signaling pathway remains operational and also stimulates IAPP's promoter activity under these adverse (ER stress) conditions (Figs. 8–9).

DISCUSSION

Previous studies revealed that, under normal physiological conditions, transcriptional and posttranscriptional mechanisms drive IAPP synthesis in pancreatic β-cells ((58), (32), (59)). However, the relative impact and the importance of transcriptional mechanisms including promoter activity in IAPP turnover in stressed pancreatic β-cells are unclear and hence were investigated here. The current study points to dynamic and transcriptionally-regulated IAPP turnover in stressed rat and human pancreatic β-cells, including the peptide's accumulation in unexpected intracellular compartments, notably the nucleus. Notwithstanding, the synthesized hIAPP accumulated in ER/Golgi- and secretory vesicles-containing cytoplasmic fractions, presumably *en route* to the plasma membrane for storage and release. High glucose- and thapsigargin-induced ER stress increased hIAPP accumulation in both nuclear and ER/Golgi fractions. EM studies confirmed IAPP accumulation in the nucleus and other non-secretory organelles suggesting its export from biosynthetic compartments and/or reuptake. Thus, two distinct hIAPP trafficking pathways, a canonical (vesicular) *en route* to the plasma membrane and non-canonical (to cell nucleus), concurrently operate in β-cells under these disparate cellular conditions. Previous studies demonstrated that plasma

membrane cholesterol and non-vesicular lipids may bind to monomeric hIAPP to regulate its transport across the plasma membrane and other endogenous membranes, thus providing an alternative transporting platform for peptide trafficking in cells (60, 61).

Further insight into the intracellular localization of hIAPP came from the high-resolution confocal microscopy studies which revealed hIAPP accumulation in DAPI-deficient nucleolar regions (62). Nucleoli are membrane-less nuclear domains in eukaryotic cells and the primary site for ribosomal RNA biogenesis (50, 51). The mammalian nucleolus has a classical tripartite structure consisting of the central-fibrillar component, middle-dense fibrillar component, and outer-granular component, each participating in specific stages of ribosomal RNA biogenesis (50, 51). In addition to the regulation of ribosomal RNA biosynthesis, (63), a recent study points to the important role of the nucleolus as a protein quality control center in cells (64). Nucleolin is a nucleolar phosphoprotein primarily localized in the dense fibrillar component of the nucleolus (65). Accumulation of hIAPP in and around the center of nucleolin-positive areas in the human islet cells strongly indicates its association with a central fibrillar component of the nucleolus. Enhanced hIAPP accumulation within the nucleolin/TIA1-positive regions of human islet β-cells evoked by ER stress or high glucose conditions suggests a possible signaling and/or regulatory role for nucleolar hIAPP in the human islet cells under these adverse conditions. Alternatively, β-cells may direct monomeric hIAPP to nucleolus for storage and/or refolding, thus adopting a recycling pathway of many other misfolded nuclear and cytosolic proteins (64). In some cells, the nucleolar aggresomes harbor aggregated proteins accumulating within or in close proximity of the nucleolus (66, 67). Nucleolar aggresomes usually consist of conjugated ubiquitin-labeled proteins and polyadenylated RNA (66). Nucleolar aggresomes can be induced by various cellular stress conditions as well as compromised protein degradation (66). Because hIAPP has a strong propensity to aggregate, it is possible that nucleolar accumulation of hIAPP, at least in part, is due to sequestration and trafficking of (mis)folded but still soluble (non-aggregating) forms of hIAPP to the nucleolus, which may reduce its toxicity. Indeed, co-staining of T2DM human islets with hIAPP specific antibody and amyloid stain, Thioflavin-T (Th-T), revealed Th-T negative hIAPP assemblies in the nuclear regions of β-cells, thus making this scenario possible. In line with this observation, cell fractionation studies revealed the accumulation of monomeric but not oligomeric hIAPP in the nucleus. Our biochemical studies further revealed that stress-induced hIAPP accumulation in the nucleus quantitatively accounts for a significant portion (~10–20%) of total hIAPP intracellular content. Interestingly, prolonged high glucose conditions or induction of ER stress co-induced expression of heat shock proteins, BIP and HSP70, as well as hIAPP in human islet β-cells, indicating their possible co-regulatory roles and function in stressed β-cells.

It has been shown that proinsulin C-peptide, a degradation fragment of proinsulin molecule, traffics to nucleoli to regulate the ribosomal rDNA transcription in cells (38). Recent studies reported that PGC1α, the master regulator of mitochondrial biogenesis, localizes to the nucleolus and regulates RNA polymerase-I transcription under various stress conditions in mouse models and humans (68). At present, the functional significance of the nucleolar localization of hIAPP is unclear. It is well established that ribosomal RNA biogenesis is tightly coordinated with cell proliferation and growth, all of which are impacted during

cellular stress (69). The previous study demonstrated that exogenous (extracellular) mouse IAPP stimulated mouse β-cell proliferation in a glucose-dependent manner by regulating Erk1 / 2 and Akt signaling cascade (70). Therefore, it is possible that nucleolar hIAPP also serves as a signaling molecule and regulates the biosynthesis of ribosomal subunits, which in turn affects the proliferative capability of β-cells. However, only a minor fraction of proliferative β–cells harbored hIAPP in the nucleolus. Importantly, knockdown of hIAPP in human islets did not alter the expression of proliferation/cell cycle markers such as Ki67, evoked by high glucose. Similarly, hIAPP knockdown or overexpression had no significant effects on precursor or mature rRNA levels suggesting that hIAPP expression is dispensable for ribosomal biosynthesis. At least in this aspect, intracellular hIAPP differs from proliferative actions of extracellular proinsulin C-peptide and mouse IAPP (38, 70). However, our study also revealed no negative impact of hIAPP nucleolar accumulation on β-cell proliferation or rRNA synthesis, suggesting that hIAPP accumulation in the nucleus may potentially serve a protective role against toxic hIAPP oligomers/aggregates that tend to accumulate in other cellular compartments such as cytoplasm or recycling organelles (Figs. 2–4).

On the other hand, intact nucleolar organization and preserved biosynthetic functions, notably RNA pol II activity, were required for hIAPP production preceding and during ER stress. In line with these findings, transient expression of FoxA2 dominant-negative (DN) form reduced hIAPP promoter activity in ER-stressed RINm5F β-cell line and primary human islet cells. Thus, activation of the FoxA2 signaling pathway, previously reported to regulate IAPP production under physiological conditions (31), is also required for hIAPP synthesis under stress conditions. In contrast to these findings, it has been reported that FoxA2 overexpression suppressed the expression of several β-cell genes including IAPP and insulin in the INS 832/13 cell line (71). Different cellular backgrounds (INS vs. primary cells used in our study) and/or transfection strategies (stable vs. transient expression of DN FoxA2 constructs in our study) may lead to a different experimental outcome in the aforementioned FoxA2 functional studies. Importantly, our data are in line with a study by Shalev and colleagues showing a positive role for FoxA2 in IAPP expression in islet β-cells (31). Interestingly, while each of HG, TG, and TN induced a significant (between 2 and 3.5 folds) increase in IAPP transcript levels respective to control human islets, they stimulated a minor and non-significant (1–1.4 folds) increase in steady-state mRNA levels of IAPP transcription factors, FoxA2 and PDX1 (Fig. 9). In line with these transcriptomics results, we previously demonstrated that HG conditions also do not significantly change protein levels of FoxA2 (44). Collectively, these results suggest that HG and ER stress agents stimulate IAPP promoter activity and transcription, at least in part, by increasing the binding of FoxA2 and possibly PDX1 to IAPP promoter without altering their steady-state expression levels. Therefore, promoter occupancy could serve as an important and limiting factor in IAPP transcription under various pathophysiological conditions, even in situations of constant expression levels of its two transcription factors. Although our study suggests that transcriptional factor FoxA2 and stress-responsive elements in hIAPP promoter play a major role in its synthesis during ER stress, we cannot rule out the possibility that ER-stress induced hIAPP synthesis is also regulated, at least in part, at the translational level. Posttranscriptional mechanisms play an important role in hIAPP production under normal

physiological conditions (58) and they may also play a regulatory role in hIAPP production in ER-stressed β-cells. In accord with this idea, potent transcriptional inhibitor, α-amanitin, despite completely disrupting nucleolar organization, only partially inhibited hIAPP synthesis in normal and ER-stressed human islets (Fig. S5).

An important question that still remains to be resolved is to which extent is a high glucose-stimulated hIAPP expression ER-stress dependent? The current and published studies clearly demonstrate that chronic HG treatment may concurrently induce ER stress and hIAPP transcription, thus supporting this scenario. Comparative transcriptomic studies (Fig. 9) revealed that HG treatment stimulated an increase in ER-stress marker BIP albeit at a reduced level compared to potent chemical ER stress inducers, TG, and TN. On other hand, mRNA levels of a metabolic and ER stress marker, TXNIP, were markedly elevated in HG and to a lesser extent in TG/TN treated islets. Further, the hIAPP expression pattern in ER-stressed β-cells strongly correlated with TXNIP transcript levels. Relatedly, a recent study by Shalev and colleagues demonstrated the important regulatory role of TXNIP in FoxA2-mediated IAPP expression in normal and HG-treated islet β-cells (31). Thus, our current study supports (or at least does not preclude) the idea that HG and ER-stress may stimulate hIAPP production via a shared TXNIP/FoxA2-signaling pathway. In line with this notion, CHIP studies showed that the binding of carbohydrate response element-binding protein (ChREBP) to the *txnip* promoter is augmented in HG and TG/TN treated β-cells, and is critically important for the enhanced TXNIP transcription under high glucose and ER-stress conditions (36, 57). However, the extent to which these TXNIP-mediated metabolic and stress pathways overlap and drive HG-induced hIAPP synthesis remains to be resolved in the future.

CONCLUSIONS

In summary, our studies revealed the involvement of a non-conventional nuclear trafficking route in hIAPP monomer turnover in β-cells that operate in parallel with canonical anterograde protein transport pathways. Nucleolar hIAPP levels were also markedly elevated in human islets procured from T2DM individuals, implying that this non-canonical trafficking pathway operates under pathological and clinically relevant conditions. Because FoxA2 and RNA Pol II are required for hIAPP synthesis and accumulation under normal and diabetes-mirroring conditions, they could serve as potential druggable targets to reduce hIAPP aggregation and toxicity in T2DM.

Supplementary Material

Refer to Web version on PubMed Central for supplementary material.

Acknowledgments

We thank NIDDK-supported Integrated Islet Distribution Program at the City of Hope for making human islets available for the present study. We thank GW Nanofabrication and Imaging Center for assistance with EM studies. We are grateful to our colleagues C. A. Brantner and A. Popratiloff for helpful comments and guidance in our EM and 3D confocal studies and image analysis. We thank C. Day and M. Joe for technical help with the design and preparation of WT and DN FoxA2 mutant promoter plasmids. We thank M. Joe for technical help in generating stable IAPP expressing β-cell lines. We also thank our colleagues Robert Donaldson and Julie Donaldson for critical reading of the manuscript and stimulating discussions on the subject

Funding

This work was supported by the National Institute of Health (grant no. RO1DK091845 to A.J.) and GWU UFF award (to A.J.).

Abbreviations

T2DM	type 2 diabetes mellitus
hIAPP	human islet amyloid polypeptide
rIAPP	rat islet amyloid polypeptide
ANOVA	analysis of variance
FoxA2	forkhead box protein A2
Glc	glucose
qPCR	quantitative PCR
IEQ	islet equivalents
DN	dominant negative
WT	wild type

REFERENCES

1. Hung MC, Link W. Protein localization in disease and therapy. J Cell Sci. 2011;124(Pt 20):3381–92. [PubMed: 22010196]
2. Mulder H, Ahren B, Sundler F. Islet amyloid polypeptide and insulin gene expression are regulated in parallel by glucose in vivo in rats. Am J Physiol. 1996;271(6 Pt 1):E1008–14. [PubMed: 8997219]
3. Butler AE, Janson J, Bonner-Weir S, Ritzel R, Rizza RA, Butler PC. Beta-cell deficit and increased beta-cell apoptosis in humans with type 2 diabetes. Diabetes. 2003;52(1):102–10. [PubMed: 12502499]
4. Mukherjee A, Morales-Scheihing D, Butler PC, Soto C. Type 2 diabetes as a protein misfolding disease. Trends Mol Med. 2015;21(7):439–49. [PubMed: 25998900]
5. Christmanson L, Rorsman F, Stenman G, Westermark P, Betsholtz C. The human islet amyloid polypeptide (IAPP) gene. Organization, chromosomal localization and functional identification of a promoter region. FEBS Lett. 1990;267(1):160–6. [PubMed: 2365085]
6. Westermark P, Andersson A, Westermark GT. Islet amyloid polypeptide, islet amyloid, and diabetes mellitus. Physiol Rev. 2011;91(3):795–826. [PubMed: 21742788]
7. Martin C. The physiology of amylin and insulin: maintaining the balance between glucose secretion and glucose uptake. Diabetes Educ. 2006;32 Suppl 3:101S–4S. [PubMed: 16751350]
8. Ling W, Huang YM, Qiao YC, Zhang XX, Zhao HL. Human Amylin: From Pathology to Physiology and Pharmacology. Curr Protein Pept Sci. 2019;20(9):944–57. [PubMed: 30919775]
9. Costes S. Targeting protein misfolding to protect pancreatic beta-cells in type 2 diabetes. Curr Opin Pharmacol. 2018;43:104–10. [PubMed: 30245473]
10. Khoo C, Yang J, Rajpal G, Wang Y, Liu J, Arvan P, et al. Endoplasmic reticulum oxidoreductin-1-like beta (ERO1lbeta) regulates susceptibility to endoplasmic reticulum stress and is induced by insulin flux in beta-cells. Endocrinology. 2011;152(7):2599–608. [PubMed: 21540283]

11. Zito E, Chin KT, Blais J, Harding HP, Ron D. ERO1-beta, a pancreas-specific disulfide oxidase, promotes insulin biogenesis and glucose homeostasis. J Cell Biol. 2010;188(6):821–32. [PubMed: 20308425]
12. Gupta S, McGrath B, Cavener DR. PERK (EIF2AK3) regulates proinsulin trafficking and quality control in the secretory pathway. Diabetes. 2010;59(8):1937–47. [PubMed: 20530744]
13. Scheuner D, Vander Mierde D, Song B, Flamez D, Creemers JW, Tsukamoto K, et al. Control of mRNA translation preserves endoplasmic reticulum function in beta cells and maintains glucose homeostasis. Nat Med. 2005;11(7):757–64. [PubMed: 15980866]
14. Haataja L, Snapp E, Wright J, Liu M, Hardy AB, Wheeler MB, et al. Proinsulin intermolecular interactions during secretory trafficking in pancreatic beta cells. J Biol Chem. 2013;288(3):1896–906. [PubMed: 23223446]
15. Kontopoulos E, Parvin JD, Feany MB. Alpha-synuclein acts in the nucleus to inhibit histone acetylation and promote neurotoxicity. Hum Mol Genet. 2006;15(20):3012–23. [PubMed: 16959795]
16. Gersbacher MT, Goodger ZV, Trutzel A, Bundschuh D, Nitsch RM, Konietzko U. Turnover of amyloid precursor protein family members determines their nuclear signaling capability. PLoS One. 2013;8(7):e69363. [PubMed: 23874953]
17. Singh S, Trikha S, Sarkar A, Jeremic AM. Proteasome regulates turnover of toxic human amylin in pancreatic cells. Biochem J. 2016;473(17):2655–70. [PubMed: 27340132]
18. Eizirik DL, Cardozo AK, Cnop M. The role for endoplasmic reticulum stress in diabetes mellitus. Endocr Rev. 2008;29(1):42–61. [PubMed: 18048764]
19. Scheuner D, Kaufman RJ. The unfolded protein response: a pathway that links insulin demand with beta-cell failure and diabetes. Endocr Rev. 2008;29(3):317–33. [PubMed: 18436705]
20. Kim MK, Kim HS, Lee IK, Park KG. Endoplasmic reticulum stress and insulin biosynthesis: a review. Exp Diabetes Res. 2012;2012:509437. [PubMed: 22474424]
21. Boyce M, Yuan J. Cellular response to endoplasmic reticulum stress: a matter of life or death. Cell Death Differ. 2006;13(3):363–73. [PubMed: 16397583]
22. Olson LK, Redmon JB, Towle HC, Robertson RP. Chronic exposure of HIT cells to high glucose concentrations paradoxically decreases insulin gene transcription and alters binding of insulin gene regulatory protein. J Clin Invest. 1993;92(1):514–9. [PubMed: 8326016]
23. Olson LK, Sharma A, Peshavaria M, Wright CV, Towle HC, Rodertson RP, et al. Reduction of insulin gene transcription in HIT-T15 beta cells chronically exposed to a supraphysiologic glucose concentration is associated with loss of STF-1 transcription factor expression. Proc Natl Acad Sci U S A. 1995;92(20):9127–31. [PubMed: 7568086]
24. Hoppener JW, Oosterwijk C, Nieuwenhuis MG, Posthuma G, Thijssen JH, Vroom TM, et al. Extensive islet amyloid formation is induced by development of Type II diabetes mellitus and contributes to its progression: pathogenesis of diabetes in a mouse model. Diabetologia. 1999;42(4):427–34. [PubMed: 10230646]
25. de Koning EJ, Bodkin NL, Hansen BC, Clark A. Diabetes mellitus in Macaca mulatta monkeys is characterised by islet amyloidosis and reduction in beta-cell population. Diabetologia. 1993;36(5):378–84. [PubMed: 8314440]
26. Narita R, Toshimori H, Nakazato M, Kuribayashi T, Toshimori T, Kawabata K, et al. Islet amyloid polypeptide (IAPP) and pancreatic islet amyloid deposition in diabetic and non-diabetic patients. Diabetes Res Clin Pract. 1992;15(1):3–14. [PubMed: 1541232]
27. Guardado-Mendoza R, Davalli AM, Chavez AO, Hubbard GB, Dick EJ, Majluf-Cruz A, et al. Pancreatic islet amyloidosis, beta-cell apoptosis, and alpha-cell proliferation are determinants of islet remodeling in type-2 diabetic baboons. Proc Natl Acad Sci U S A. 2009;106(33):13992–7. [PubMed: 19666551]
28. Singh S, Bhowmick DC, Pany S, Joe M, Zaghlula N, Jeremic AM. Apoptosis signal regulating kinase-1 and NADPH oxidase mediate human amylin evoked redox stress and apoptosis in pancreatic beta-cells. Biochim Biophys Acta Biomembr. 2018.
29. Shalev A, Pise-Masison CA, Radonovich M, Hoffmann SC, Hirshberg B, Brady JN, et al. Oligonucleotide microarray analysis of intact human pancreatic islets: identification of glucose-

responsive genes and a highly regulated TGFbeta signaling pathway. Endocrinology. 2002;143(9):3695–8. [PubMed: 12193586]

30. Gasa R, Gomis R, Casamitjana R, Novials A. Signals related to glucose metabolism regulate islet amyloid polypeptide (IAPP) gene expression in human pancreatic islets. Regul Pept. 1997;68(2):99–104. [PubMed: 9110380]
31. Jing G, Westwell-Roper C, Chen J, Xu G, Verchere CB, Shalev A. Thioredoxin-interacting protein promotes islet amyloid polypeptide expression through miR-124a and FoxA2. J Biol Chem. 2014;289(17):11807–15. [PubMed: 24627476]
32. Macfarlane WM, Campbell SC, Elrick LJ, Oates V, Bermano G, Lindley KJ, et al. Glucose regulates islet amyloid polypeptide gene transcription in a PDX1- and calcium-dependent manner. J Biol Chem. 2000;275(20):15330–5. [PubMed: 10748090]
33. Watada H, Kajimoto Y, Kaneto H, Matsuoka T, Fujitani Y, Miyazaki J, et al. Involvement of the homeodomain-containing transcription factor PDX-1 in islet amyloid polypeptide gene transcription. Biochem Biophys Res Commun. 1996;229(3):746–51. [PubMed: 8954967]
34. Wang M, Drucker DJ. Activation of amylin gene transcription by LIM domain homeobox gene isl-1. Mol Endocrinol. 1996;10(3):243–51. [PubMed: 8833653]
35. Lee S, Min Kim S, Dotimas J, Li L, Feener EP, Baldus S, et al. Thioredoxin-interacting protein regulates protein disulfide isomerases and endoplasmic reticulum stress. EMBO Mol Med. 2014;6(6):732–43. [PubMed: 24843047]
36. Oslowski CM, Hara T, O'Sullivan-Murphy B, Kanekura K, Lu S, Hara M, et al. Thioredoxin-interacting protein mediates ER stress-induced beta cell death through initiation of the inflammasome. Cell Metab. 2012;16(2):265–73. [PubMed: 22883234]
37. Xu G, Chen J, Jing G, Shalev A. Thioredoxin-interacting protein regulates insulin transcription through microRNA-204. Nat Med. 2013;19(9):1141–6. [PubMed: 23975026]
38. Lindahl E, Nyman U, Zaman F, Palmberg C, Cascante A, Shafqat J, et al. Proinsulin C-peptide regulates ribosomal RNA expression. J Biol Chem. 2010;285(5):3462–9. [PubMed: 19917601]
39. Prieto C, Fontana D, Etcheverrigaray M, Kratje R. A strategy to obtain recombinant cell lines with high expression levels. Lentiviral vector-mediated transgenesis. BMC Proc. 2011;5 Suppl 8:P7. [PubMed: 22373510]
40. Salic A, Mitchison TJ. A chemical method for fast and sensitive detection of DNA synthesis in vivo. Proc Natl Acad Sci U S A. 2008;105(7):2415–20. [PubMed: 18272492]
41. Inwald EC, Klinkhammer-Schalke M, Hofstadter F, Zeman F, Koller M, Gerstenhauer M, et al. Ki-67 is a prognostic parameter in breast cancer patients: results of a large population-based cohort of a cancer registry. Breast Cancer Res Treat. 2013;139(2):539–52. [PubMed: 23674192]
42. Gerdes J, Lemke H, Baisch H, Wacker HH, Schwab U, Stein H. Cell cycle analysis of a cell proliferation-associated human nuclear antigen defined by the monoclonal antibody Ki-67. J Immunol. 1984;133(4):1710–5. [PubMed: 6206131]
43. Scholzen T, Gerdes J. The Ki-67 protein: from the known and the unknown. J Cell Physiol. 2000;182(3):311–22. [PubMed: 10653597]
44. Chatterjee Bhowmick D, Jeremic A. Functional proteasome complex is required for turnover of islet amyloid polypeptide in pancreatic beta-cells. J Biol Chem. 2018;293(37):14210–23. [PubMed: 30012886]
45. Magzoub M, Miranker AD. Concentration-dependent transitions govern the subcellular localization of islet amyloid polypeptide. FASEB J. 2012;26(3):1228–38. [PubMed: 22183778]
46. Birol M, Kumar S, Rhoades E, Miranker AD. Conformational switching within dynamic oligomers underpins toxic gain-of-function by diabetes-associated amyloid. Nat Commun. 2018;9(1):1312. [PubMed: 29615609]
47. Rivera JF, Gurlo T, Daval M, Huang CJ, Matveyenko AV, Butler PC, et al. Human-IAPP disrupts the autophagy/lysosomal pathway in pancreatic beta-cells: protective role of p62-positive cytoplasmic inclusions. Cell Death Differ. 2011;18(3):415–26. [PubMed: 20814419]
48. Gurlo T, Ryazantsev S, Huang CJ, Yeh MW, Reber HA, Hines OJ, et al. Evidence for proteotoxicity in beta cells in type 2 diabetes: toxic islet amyloid polypeptide oligomers form intracellularly in the secretory pathway. Am J Pathol. 2010;176(2):861–9. [PubMed: 20042670]

49. Lutz TA, Meyer U. Amylin at the interface between metabolic and neurodegenerative disorders. Front Neurosci. 2015;9:216. [PubMed: 26136651]
50. Boisvert FM, van Koningsbruggen S, Navascues J, Lamond AI. The multifunctional nucleolus. Nat Rev Mol Cell Biol. 2007;8(7):574–85. [PubMed: 17519961]
51. Hernandez-Verdun D, Roussel P, Thiry M, Sirri V, Lafontaine DL. The nucleolus: structure/function relationship in RNA metabolism. Wiley Interdiscip Rev RNA. 2010;1(3):415–31. [PubMed: 21956940]
52. Hasnain SZ, Prins JB, McGuckin MA. Oxidative and endoplasmic reticulum stress in beta-cell dysfunction in diabetes. J Mol Endocrinol. 2016;56(2):R33–54. [PubMed: 26576641]
53. Huang G, Yao J, Zeng W, Mizuno Y, Kamm KE, Stull JT, et al. ER stress disrupts Ca2+-signaling complexes and Ca2+ regulation in secretory and muscle cells from PERK-knockout mice. J Cell Sci. 2006;119(Pt 1):153–61. [PubMed: 16352659]
54. Caudron-Herger M, Pankert T, Seiler J, Nemeth A, Voit R, Grummt I, et al. Alu element-containing RNAs maintain nucleolar structure and function. EMBO J. 2015;34(22):2758–74. [PubMed: 26464461]
55. Han Z, Alves C, Gudima S, Taylor J. Intracellular localization of hepatitis delta virus proteins in the presence and absence of viral RNA accumulation. J Virol. 2009;83(13):6457–63. [PubMed: 19369324]
56. Luo B, Li B, Wang W, Liu X, Xia Y, Zhang C, et al. NLRP3 gene silencing ameliorates diabetic cardiomyopathy in a type 2 diabetes rat model. PLoS One. 2014;9(8):e104771. [PubMed: 25136835]
57. Cha-Molstad H, Saxena G, Chen J, Shalev A. Glucose-stimulated expression of Txnip is mediated by carbohydrate response element-binding protein, p300, and histone H4 acetylation in pancreatic beta cells. J Biol Chem. 2009;284(25):16898–905. [PubMed: 19411249]
58. Alarcon C, Verchere CB, Rhodes CJ. Translational control of glucose-induced islet amyloid polypeptide production in pancreatic islets. Endocrinology. 2012;153(5):2082–7. [PubMed: 22408171]
59. Shepherd LM, Campbell SC, Macfarlane WM. Transcriptional regulation of the IAPP gene in pancreatic beta-cells. Biochim Biophys Acta. 2004;1681(1):28–37. [PubMed: 15566941]
60. Trikha S, Jeremic AM. Clustering and internalization of toxic amylin oligomers in pancreatic cells require plasma membrane cholesterol. J Biol Chem. 2011;286(41):36086–97. [PubMed: 21865171]
61. Scollo F, Tempra C, Lolicato F, Sciacca MFM, Raudino A, Milardi D, et al. Phospholipids Critical Micellar Concentrations Trigger Different Mechanisms of Intrinsically Disordered Proteins Interaction with Model Membranes. J Phys Chem Lett. 2018;9(17):5125–9. [PubMed: 30133296]
62. Sirri V, Urcuqui-Inchima S, Roussel P, Hernandez-Verdun D. Nucleolus: the fascinating nuclear body. Histochem Cell Biol. 2008;129(1):13–31. [PubMed: 18046571]
63. Boulon S, Westman BJ, Hutten S, Boisvert FM, Lamond AI. The nucleolus under stress. Mol Cell. 2010;40(2):216–27. [PubMed: 20965417]
64. Frottin F, Schueder F, Tiwary S, Gupta R, Korner R, Schlichthaerle T, et al. The nucleolus functions as a phase-separated protein quality control compartment. Science. 2019;365(6451):342–7. [PubMed: 31296649]
65. Tajrishi MM, Tuteja R, Tuteja N. Nucleolin: The most abundant multifunctional phosphoprotein of nucleolus. Commun Integr Biol. 2011;4(3):267–75. [PubMed: 21980556]
66. Latonen L. Nucleolar aggresomes as counterparts of cytoplasmic aggresomes in proteotoxic stress. Proteasome inhibitors induce nuclear ribonucleoprotein inclusions that accumulate several key factors of neurodegenerative diseases and cancer. Bioessays. 2011;33(5):386–95. [PubMed: 21425306]
67. Klibanov SA, O'Hagan HM, Ljungman M. Accumulation of soluble and nucleolar-associated p53 proteins following cellular stress. J Cell Sci. 2001;114(Pt 10):1867–73. [PubMed: 11329373]
68. Jesse S, Bayer H, Alupei MC, Zugel M, Mulaw M, Tuorto F, et al. Ribosomal transcription is regulated by PGC-1alpha and disturbed in Huntington's disease. Sci Rep. 2017;7(1):8513. [PubMed: 28819135]

69. Lempiainen H, Shore D. Growth control and ribosome biogenesis. Curr Opin Cell Biol. 2009;21(6):855–63. [PubMed: 19796927]

70. Visa M, Alcarraz-Vizan G, Montane J, Cadavez L, Castano C, Villanueva-Penacarrillo ML, et al. Islet amyloid polypeptide exerts a novel autocrine action in beta-cell signaling and proliferation. FASEB J. 2015;29(7):2970–9. [PubMed: 25808537]

71. Wang H, Gauthier BR, Hagenfeldt-Johansson KA, Iezzi M, Wollheim CB. Foxa2 (HNF3beta) controls multiple genes implicated in metabolism-secretion coupling of glucose-induced insulin release. J Biol Chem. 2002;277(20):17564–70. [PubMed: 11875061]

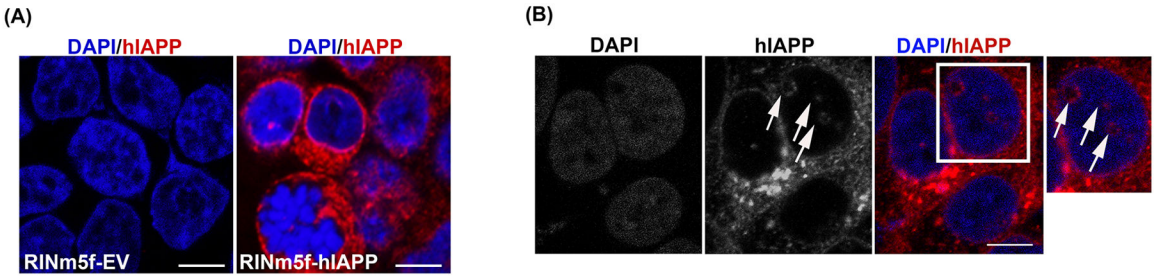

Figure 1. hIAPP trafficking routes in RIN-m5f cells.

RIN-m5f cells were transduced with empty vector (EV), hIAPP or rIAPP encoding lentivirus particles for 48h. (A) Immuno-confocal microscopy optical section (1μm-Z plane) of RIN-m5f cells transduced with empty vector (EV) and hIAPP encoding lentivirus. Cells were co-stained with hIAPP-specific IAPP monoclonal antibody (red) and DAPI (blue). (B) Representative single (1μm-Z plane) fluorescence confocal sections of hIAPP intracellular accumulation sites in hIAPP lentivirus-transduced cells. Arrows denote hIAPP's nuclear locations in micrographs. Bars, 5μm.

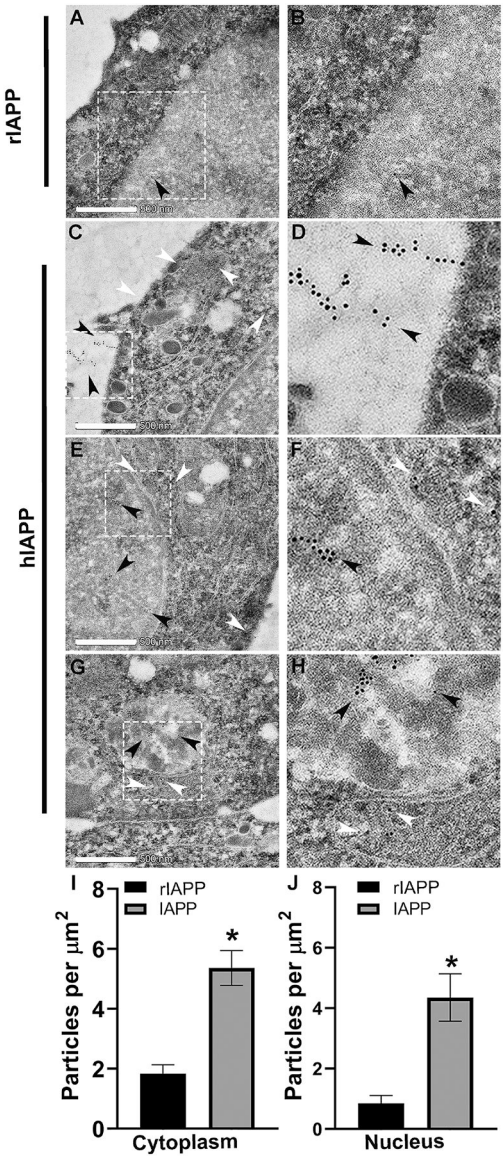

Figure 2. TEM analysis of IAPP trafficking in rat insulinoma cells.

Synchronized control (rIAPP) and hIAPP-expressing rat insulinoma (INS 832/13) cells were harvested and processed for TEM analysis as described in material and methods. (A-B) Control rat INS 832/13 cells were examined for rat IAPP intracellular distribution. Representative EM image depicts rat IAPP immuno-localization in the nucleus (arrowhead) of control cells. (C-D) EM analysis revealed secretion and extracellular accumulation of immuno-gold conjugated hIAPP antibodies in hIAPP-expressing cells (depicted by black arrowheads). (E-F) TEM shows nuclear (black arrowheads) and cytosolic (white arrowheads) accumulation of IAPP in hIAPP-expressing cells. (G-H) hIAPP was also found in the mitochondria (white arrowheads) and autophagosomes (black arrowheads). (I, J) Immuno-quantitative analysis of IAPP accumulation in the nucleus and cytosolic compartments of control (rIAPP-expressing, black) and stable hIAPP-expressing (gray) INS

832/13 cells. *p<0.05, Student's t-test. Magnified areas in original images (white box) are presented on the right. Bar, 500 nm.

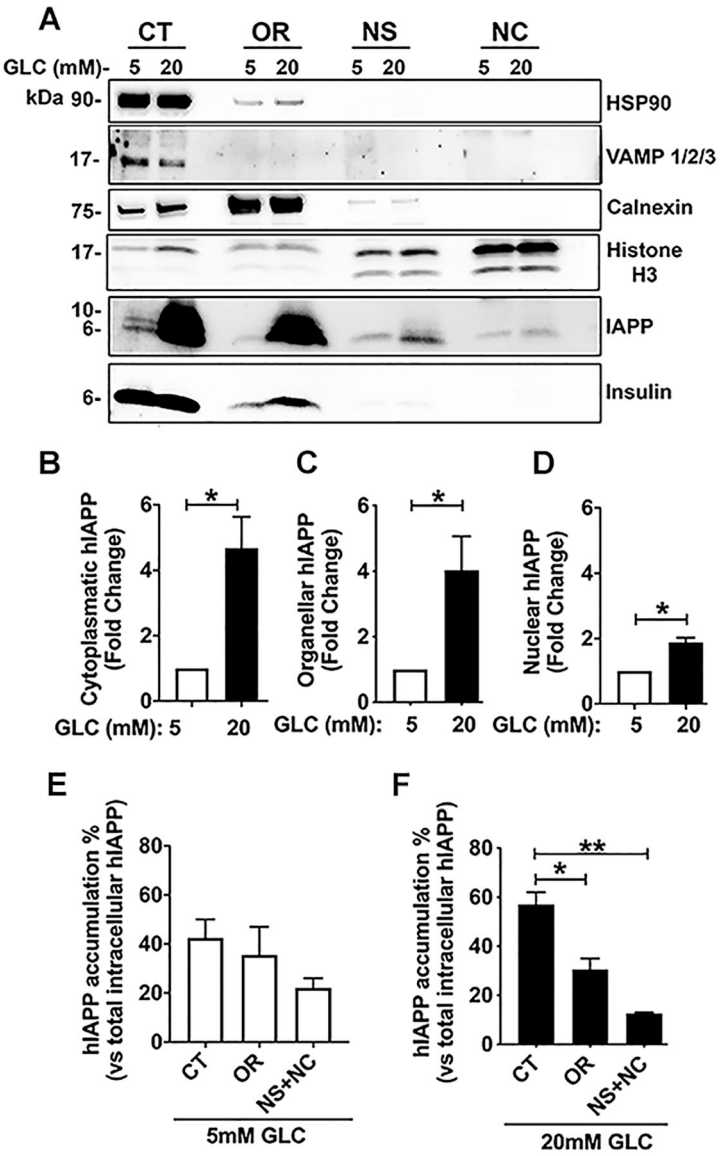

Figure 3. Biochemical analysis of IAPP trafficking in human islet cells.

Human islets were cultured in basal (5mM) and high glucose (20mM) media for 4 days, followed by cell fractionation as described in the method section. (A) Western blot analysis of insulin and hIAPP distribution within the main cellular compartments under the basal and stress (high glucose) conditions. The following organelle-specific marker protein antibodies were used to determine hIAPP and insulin distribution within subcellular fractions: CT, the cytoplasmic fraction (HSP90 and VAMP), OR, ER-enriched organelle fraction (calnexin), and NC, the chromatin-bound fraction (histone). (B-F) The densitometric analysis of hIAPP accumulation in the enriched fractions of cultured human islets. Significance was established at *p< 0.05, **p< 0.01, ANOVA followed by Tukey's post hoc comparison test. Data represent mean ± SEM of three independent experiments.

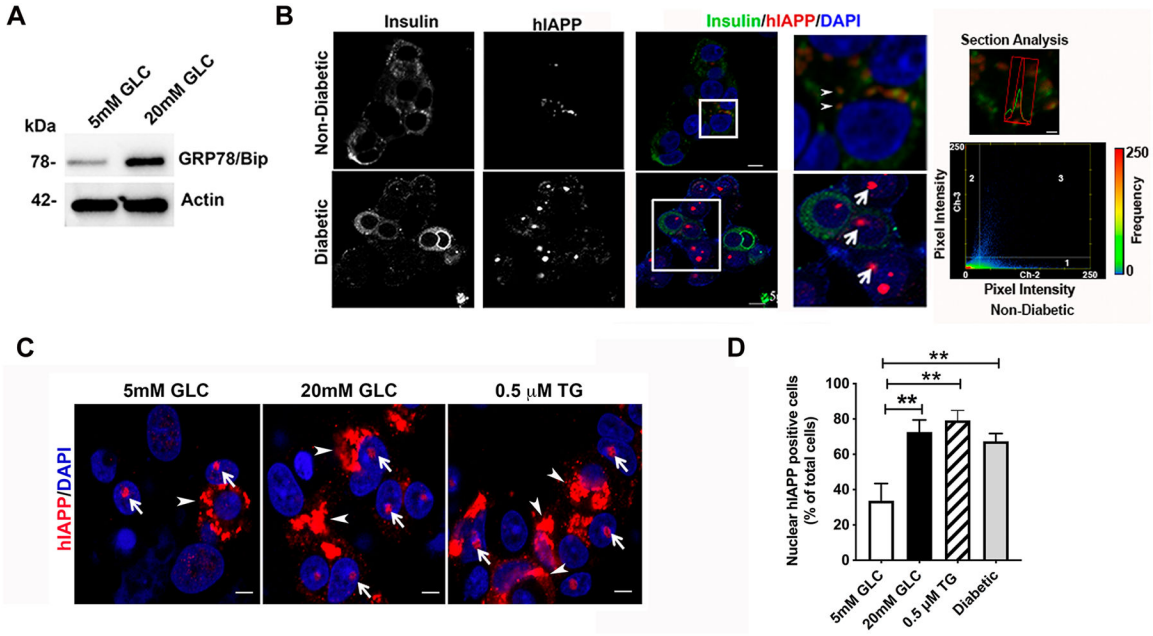

Figure 4. Nuclear accumulation of hIAPP in T2DM and ER stressed human islets.

Non-diabetic human islets were cultured in basal (5mM) and high glucose (20mM) media for 4 days or with the ER stress inducer thapsigargin (0.5μM) for 24 h. (A) Western blot analysis of ER stress marker protein GRP78 (BiP) expression in human islets. (B) Immuno-confocal microscopy analysis of hIAPP and insulin protein distribution in control non-diabetic and T2DM human islets. Cells were co-stained with hIAPP-specific IAPP monoclonal antibody (red), nuclear dye, DAPI (blue) and insulin (green). Bar, 5 μm. In magnified images on the right, arrows point to hIAPP assemblies in the cell nuclei. Arrowheads denote submicron-sized cytoplasmic vesicles containing hIAPP and insulin. An overlap between hIAPP (red trace) and insulin (green trace) fluorescence signals were detected with section analysis (Bar, 1 μm). Colocalization analysis was performed with ZEN software. Every pixel in the image was plotted in the scatterplot based on its intensity level from each channel. The pseudo-color in the scatterplot represents the number of pixels from individual channels (quadrants 1 and 2) and colocalized pixels (quadrant 3). Insulin (Ch-2) intensity distribution is shown on the x-axis and hIAPP (Ch-3) intensity distribution is shown on the y-axis. The lower left (unlabeled) quadrant in the scatterplot represents background pixels that have low intensity levels in both channels, which were excluded from colocalization analysis. (C) Quantitative immuno-confocal microscopy analysis of hIAPP nuclear expression under normal and ER stress conditions evoked by high glucose (20mM) or thapsigargin (0.5μM, 24h). Cells were co-stained with hIAPP-specific IAPP monoclonal antibody (red) and nuclear dye, DAPI (blue). Arrows and arrowheads denote nuclear and cytoplasmic hIAPP assemblies in the micrographs, respectively. Bar, 5μm. (D) Quantitative analysis of the nuclear hIAPP positive cells in the non-diabetic and T2DM human islets. Significance established at ** $p < 0.01$, ANOVA followed by Tukey's post hoc comparison test. Data represent mean ± SEM of three independent experiments.

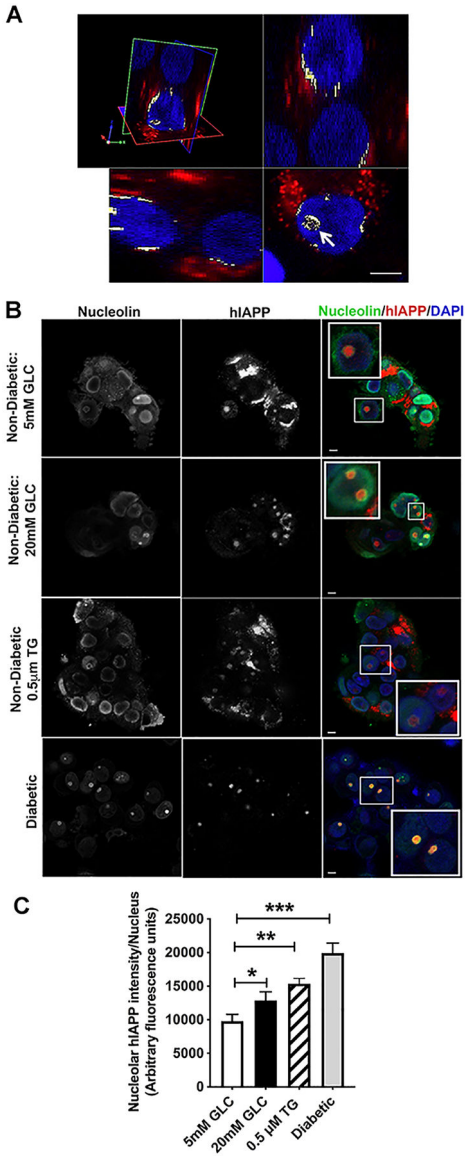

Figure 5. Cellular stress stimulates hIAPP trafficking to the nucleolus.

Non-diabetic human islets were cultured for 4 days in basal (5mM) or high glucose (20mM) media, or with ER stress inducer thapsigargin (0.5μM) for 24 h, and hIAPP trafficking and accumulation examined by immuno-confocal microscopy. (A) 3D immuno-confocal analysis reveals hIAPP-positive puncta in nucleolar and perinuclear regions (white) of cultured human islets. Cells were co-stained with the hIAPP-specific monoclonal antibody (red) and nuclear dye, DAPI (blue). Arrow points to hIAPP-signal within the cell nucleolus. Bar, 5μm. (B) Immuno-confocal analysis of hIAPP and nucleolar marker protein, nucleolin, distributions in control (5mM GLC), ER-stressed (20 mM GLC, 0.5 μM Thapsigargin) and confirmed type-2 diabetic human islets. Cells were co-stained with the hIAPP-specific monoclonal antibody (red), nuclear dye DAPI (blue) and nucleolin specific antibodies (green). Bar, 5μm. (C) Quantitative analysis of the nucleolar hIAPP signal in non-diabetic and T2DM human islets. Significance was established at *p< 0.05, **p< 0.01, ***p< 0.001,

ANOVA followed by Tukey's post hoc comparison test. Data represent mean ± SEM of three independent experiments.

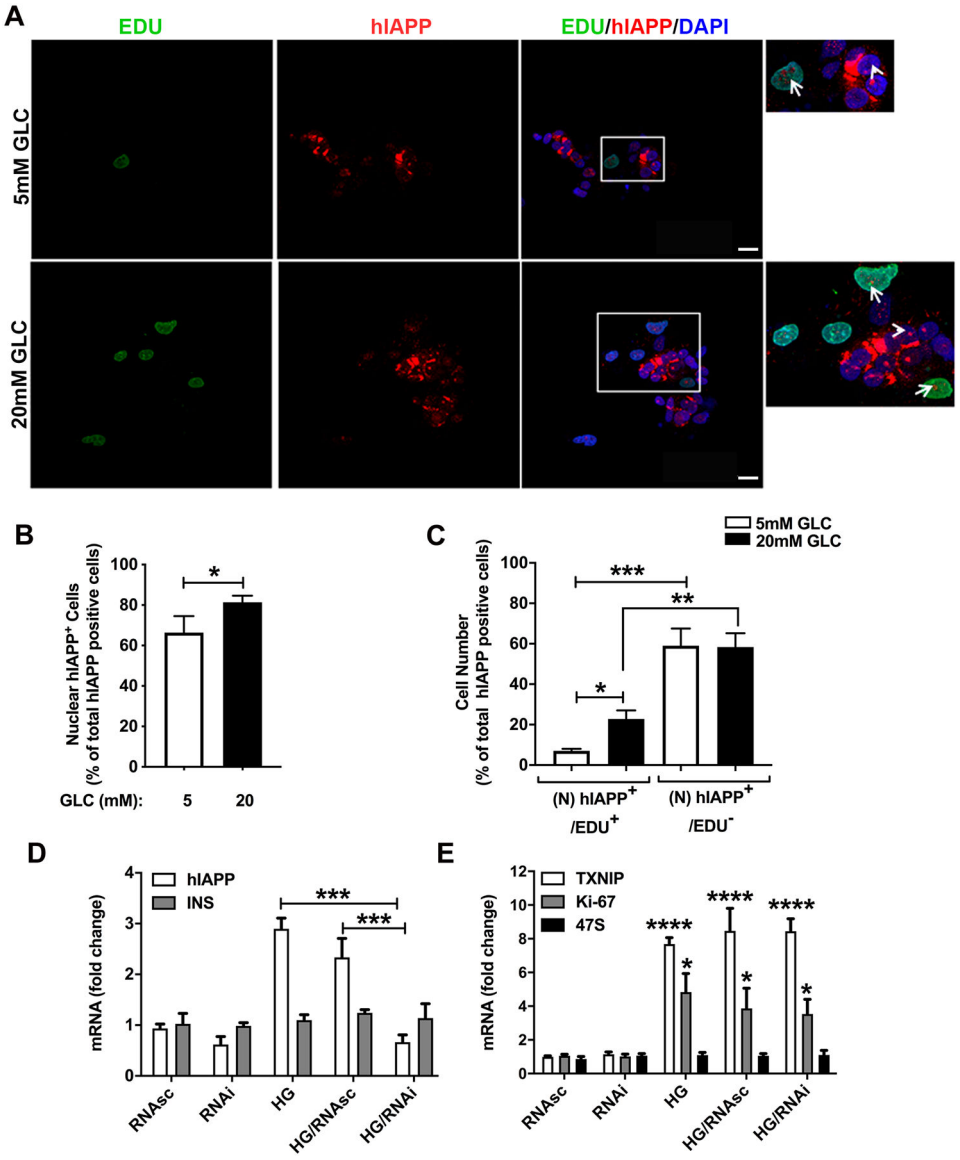

Figure 6. Effect of high glucose on hIAPP nuclear accumulation, islet cell proliferation and rRNA synthesis.

Non-diabetic human islets were cultured in basal (5mM) or high glucose (20mM) media for 4 days to stimulate hIAPP synthesis and cell proliferation. Islets were fixed, and hIAPP- and EDU-immunostaining performed to detect proliferative hIAPP-expressing islet cells. (A-C) Quantitative immuno-confocal microscopy analysis of hIAPP expression in EDU-positive (green) and non-proliferative human islet cells. Human islets were co-stained with hIAPP-specific IAPP monoclonal antibody (red) and nuclear dye, DAPI (blue). Arrows (insets) show nucleolar accumulation of hIAPP in EDU-positive islet cells. Arrowheads denote the nucleolar hIAPP signal in EDU-negative cells. Bar, 5 μm. Quantitative microscopy analysis of nuclear hIAPP expressing cells (B), and proliferative (EDU^+) and non-proliferative (EDU^-) hIAPP-expressing islet cells under basal and high glucose conditions. (C). (D-E) Effect of high glucose on expression of hIAPP and other genes in control and hIAPP-knockdown islets. Partially dissociated human islets were incubated with 40 nM of antisense or control

(scrambled) hIAPP siRNA oligonucleotide-containing transfection media. hIAPP and other gene mRNA levels were quantified in controls and treatments 48 hours post-transfection using qRT-PCR. Significance was established at **p< 0.01, ***p< 0.001, and ****p< 0.0001, ANOVA followed by Tukey's post hoc comparison test. Data represent mean ± SEM of three independent experiments.

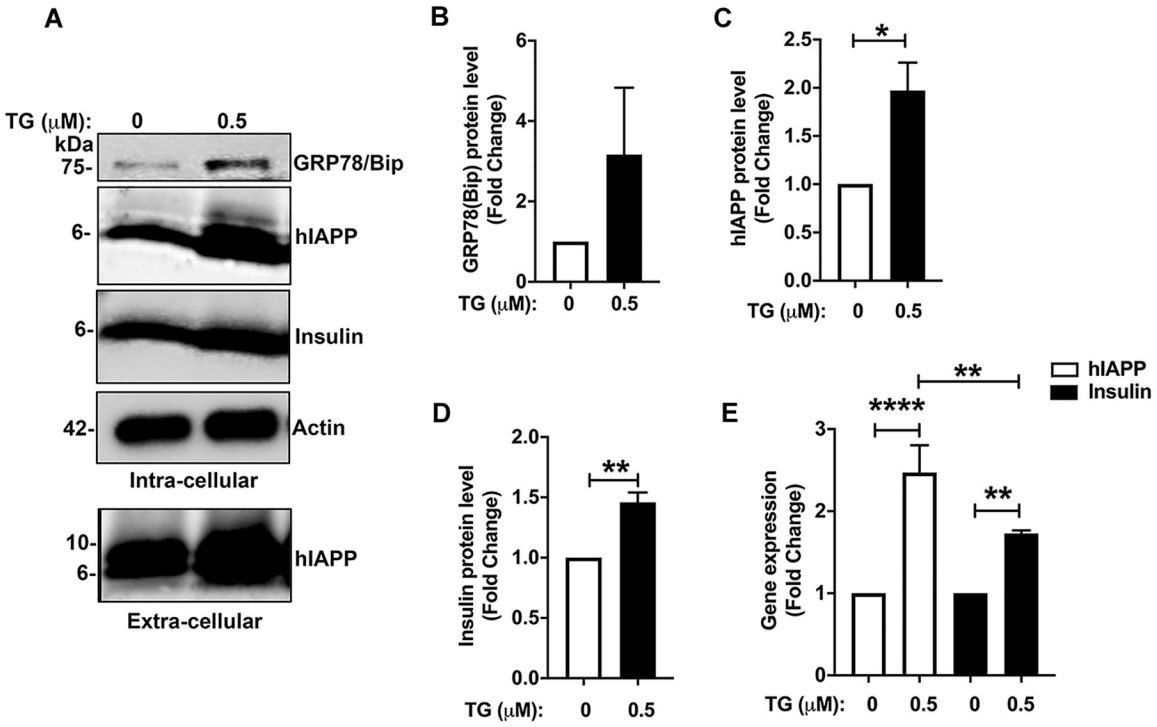

Figure 7. hIAPP mRNA and protein levels in ER-stressed β-cells.

Non-diabetic human islets were cultured in the presence or absence of 0.5 μM thapsigargin (TG) for 24h and hIAPP transcript and protein levels analyzed by RT-qPCR and western blot, respectively. (A-D) Equal protein content (10 μg) of islet cell extracts and equal volume (15μl) of culturing medium after 24h of incubation were resolved on SDS-PAGE and hIAPP protein intracellular and extracellular content analyzed by western blot and densitometry. (E) Gene (mRNA) expression analysis of the effect of ER stress on hIAPP and insulin transcription in cultured human islets. Significance was established at *p< 0.05, **p< 0.01, ***p< 0.001, ANOVA followed by Tukey's post hoc comparison test. Data represent mean ± SEM of three independent experiments.

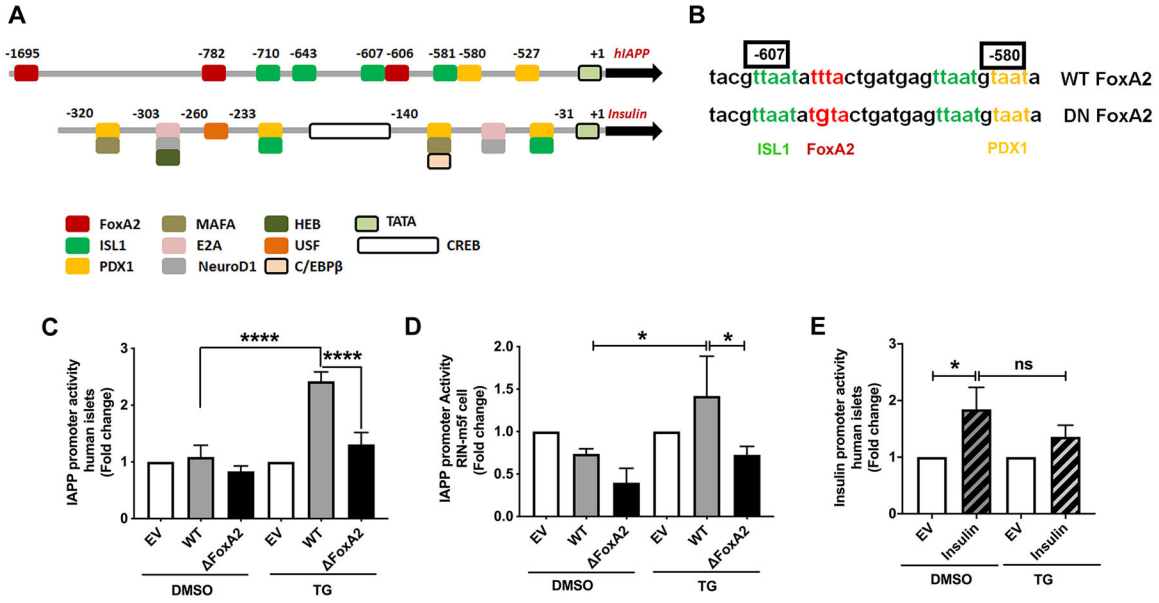

Figure 8. hIAPP promoter activation in ER-stressed pancreatic cells requires a functional FoxA2 binding site.

Freshly isolated human islet or RIN-m5F cells were co-incubated for 24h with renilla (for normalization) and firefly encoding luminescence constructs containing native (WT), mutated FoxA2 (ΔFoxA2) IAPP or WT insulin promoter. Thereafter, transfected cells were incubated with vehicle (DMSO) or 0.5 μm thapsigargin (TG) for an additional 24h. (A) Diagram depicts main transcriptional regulatory sites in hIAPP and insulin promoters. (B) Sequence alignment of WT and DN FoxA2 constructs. Mutated FoxA2 binding site within the hIAPP promoter is shown in red. (C-E) Quantification of insulin and IAPP promoter activity in control (DMSO) and ER stressed (TG) pancreatic cells. Normalized luminescence signal, reflecting promoter activity, is expressed as fold change from empty vector (EV)-transfected islets (set to 1), as described in the method section. Significance was established at *p< 0.05, and ****p< 0.0001, ANOVA followed by Tukey's post hoc comparison test. Data represent mean ± SEM of three independent experiments.

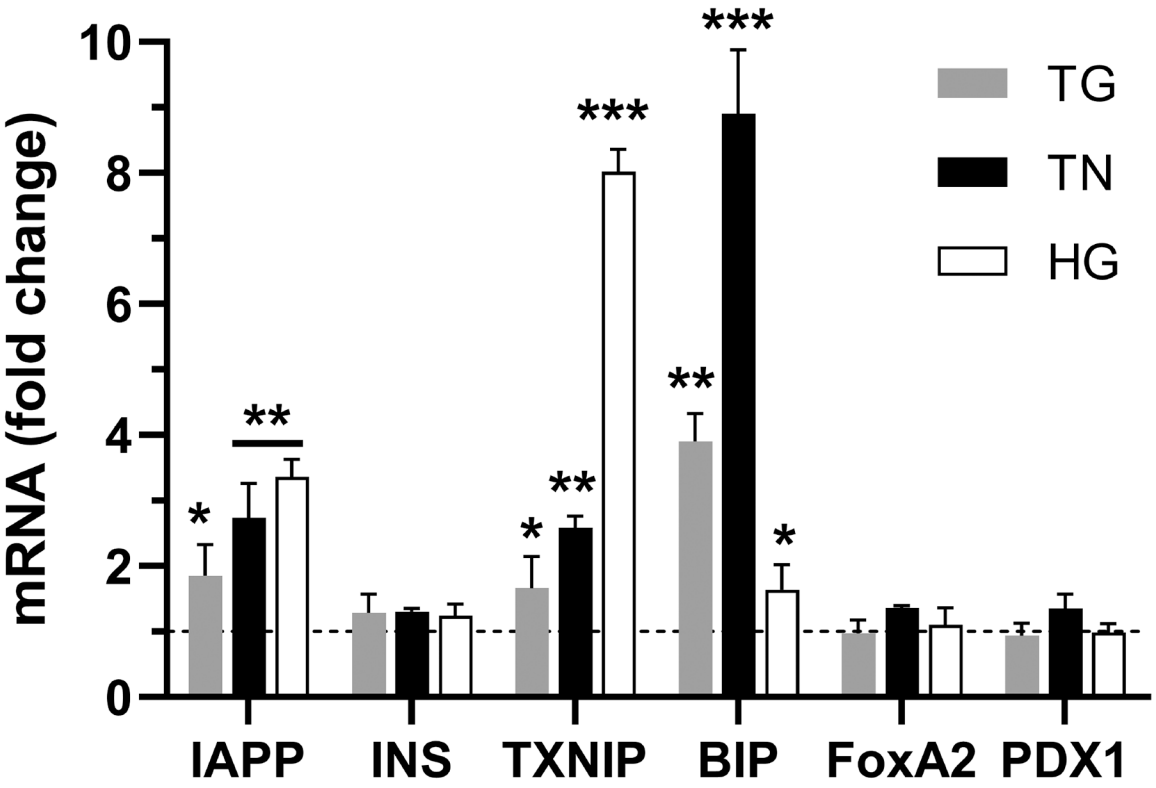

Figure 9. Transcriptomic analysis of normal and stressed cultured human islets.

Freshly isolated non-diabetic human islets were cultured in the presence of high (20mM) glucose (HG), 0.5 μM thapsigargin (TG), or 0.5 μM tunicamycin (TN) for 24h. Changes in mRNA levels of various genes analyzed by RT-qPCR. Cq values, reflecting mRNA levels, were normalized to a housekeeping gene (actin) and relative gene expression was calculated as described in the method section. Line denotes baseline gene expression in control islets. Significance was established at *p< 0.05, **p< 0.01, ***p< 0.001, ANOVA followed by Tukey's post hoc comparison test. Data represent mean ± SEM of three independent experiments.